

Light Water Reactor Sustainability Program

Nuclear Power Plant Mechanical Component Flooding Fragility Experiments FY-2017 Report



September 2017

DOE Office of Nuclear Energy

DISCLAIMER

This information was prepared as an account of work sponsored by an agency of the U.S. Government. Neither the U.S. Government nor any agency thereof, nor any of their employees, makes any warranty, expressed or implied, or assumes any legal liability or responsibility for the accuracy, completeness, or usefulness, of any information, apparatus, product, or process disclosed, or represents that its use would not infringe privately owned rights. References herein to any specific commercial product, process, or service by trade name, trade mark, manufacturer, or otherwise, does not necessarily constitute or imply its endorsement, recommendation, or favoring by the U.S. Government or any agency thereof. The views and opinions of authors expressed herein do not necessarily state or reflect those of the U.S. Government or any agency thereof.

Light Water Reactor Sustainability Program

Nuclear Power Plant Mechanical Component Flooding Fragility Experiments FY17 Report

**C. L. Pope – Idaho State University
B. Savage – Idaho State University
B. Johnson – Idaho State University
C. Muchmore – Idaho State University
L. Nichols – Idaho State University
G. Roberts – Idaho State University
E. Ryan – Idaho State University
S. Suresh – Idaho State University
A. Tahhan – Idaho State University
R. Tuladhar – Idaho State University
A. Wells – Idaho State University
C. L. Smith – Idaho National Laboratory**

September 2017

**Idaho National Laboratory
Idaho Falls, Idaho 83415
<http://www.inl.gov/lwrs>**

**Prepared for the
U.S. Department of Energy
Office of Nuclear Energy
Under DOE Idaho Operations Office
Contract DE-AC07-05ID14517**

ABSTRACT

This report describes FY17 progress on Nuclear Power Plant mechanical component flooding fragility experiments and supporting research. The progress includes execution of full scale component fragility experiments, design and implementation of improvements to the Portal Evaluation Tank, experiment design exploiting the improved Portal Evaluation Tank capabilities, fragility mathematical model development, Smoothed Particle Hydrodynamic simulations and RAVEN coupling, wave impact simulation device design, and pipe rupture mechanics research. Additionally, a component flooding experiments steering committee charter was developed and initial committee member invitations were issued. Various laboratory tours also occurred including a tour for the Idaho State Board of Education.

CONTENTS

ABSTRACT.....	iii
FIGURES.....	v
TABLES.....	vii
ACRONYMS.....	viii
1. INTRODUCTION.....	1
2. FULL-SCALE EXPERIMENTS.....	1
3. BAYESIAN REGRESSION FRAGILITY MODEL.....	5
4. PET CAPABILITY IMPROVEMENTS.....	10
5. TESTING PLANS.....	18
6. STEERING COMMITTEE CHARTER.....	18
7. SMOOTHED PARTICLE HYDRODYNAMICS.....	20
8. WAVE IMPACT SIMULATION DEVICE DESIGN.....	35
9. PIPE LEAK RESEARCH.....	45
10. CONCLUSION.....	49
11. REFERENCES.....	49

FIGURES

Figure 1. Initial PET piping configuration.....	2
Figure 2. Water depth of test 0.....	3
Figure 3. Water depth of tests 1 and 2.	4
Figure 4. Water depth of tests 3 and 4.	5
Figure 5. Improved PET piping configuration.....	11
Figure 6. Existing 12-in pipe flanging with new piping installed.....	11
Figure 7. PET high flow piping.	12
Figure 8. New PET pipe flange, inside (left) and outside (right).....	13
Figure 9. PET stand pipe for 12-in line.....	14
Figure 10. Existing 12 in flow meter (top) and 8 in flow meter (bottom).	15
Figure 11. PET downstream piping bifurcations, flow meters, and control valves.	16
Figure 12. Acrylic sheeting splash guard.....	17
Figure 13. Component Flooding Evaluation Steering Committee Charter.....	19
Figure 14. Neutrino model configuration.	21
Figure 15. Low flow rate width parametric study plot.....	22
Figure 16. High flow rate width parametric study plot.....	23
Figure 17. Low flow rate particle diameter parametric study plot.....	24
Figure 18. High flow rate particle diameter parametric study plot.	25
Figure 19. Low flow rate model width check plot.	26
Figure 20. High flow rate model width check plot.	26
Figure 21. Water elevation vs. time plot.....	27
Figure 22. Water elevation standard deviation vs. time plot.....	28
Figure 23. Total head vs. flow rate plot.	29
Figure 24. Total head relative percent error vs. flow rate plot.....	30
Figure 25: Neutrino/RAVEN coupling test simulation setup.	31
Figure 26: Neutrino/RAVEN coupling test plot.	32
Figure 27. Initial sequence of force driven door failure experiment.....	33
Figure 28. Failure of the first door after 4000 N was exerted by the build-up of particles behind it.....	34
Figure 29. Failure of the second door showing the change from static to dynamic object type.	35
Figure 30. 20 ft solitary wave Flow-3D simulation (X-Z Plane).....	37
Figure 31. Isometric view of wave pressures at imminent baffle impact.	37
Figure 32. Design F isometric view.....	38
Figure 33. Design F gate system: isometric view.	39

Figure 34. Design F isometric view: wave section profile.....	39
Figure 35. Design J isometric view.....	40
Figure 36. Design J isometric view: wave section.....	40
Figure 37. Scaled model of system with gate closed (power to electromagnet on).....	42
Figure 38. Scaled model of system with gate open (power to electromagnet off).....	43
Figure 39. Section of WISD - Inlet angle of 45 degrees and a fluid depth of 1 foot.....	44
Figure 40. Section of WISD - Inlet angle 25 degrees and a fluid depth of 2 feet.....	44
Figure 41. Mass flux vs time.....	45
Figure 42. Leak rates for normally distributed crack morphology variables [10].	47

TABLES

Table 1. Door Test Data	6
Table 2. OpenBUGS Script for Depth Model.....	7
Table 3. Results of the Depth Model	7
Table 4. Models Responses to Link Function.....	8
Table 5. Errors Observed While Using Different Link Functions	8
Table 6. Information on DIC and Other Parameters of the Seven Models	9
Table 7 Hypothetical Door Test Data	10
Table 8. Width Parametric Study Results	22
Table 9. Particle Diameter Parametric Study Results	24
Table 10. Model Width Check Results	25
Table 11. SPH Result Details.....	28
Table 12. SPH and physical results for total head and flow rate comparison.....	29
Table 13. Physical Modeling Parameters.....	41
Table 14. Various simulations conducted in FLOW 3D.....	43
Table 15. Variable Pressure Boundary	45
Table 16. SKI Report, Number of Piping Failures for Various Pipe Sizes and Pipe Size Categories [11]	48
Table 17. SKI Report, Number of Piping failures by Type of Failure [11]	48
Table 18. SKI Report, Number by Piping Failures for Each Failure Mechanism Category [11]	49

ACRONYMS

BIC	Bayesian Information Criteria
CFD	Computational Fluid Dynamics
CFEL	Component Flooding Evaluation Lab
DIC	Deviance Information Criteria
EC	Erosion/Corrosion
FV	Fatigue-Vibration
LBB	Leak Before Break
LER	Licensing Event Reports
MCMC	Markov Chain Monte Carlo
NPP	Nuclear Power Plant
PET	Portal Evaluation Tank
RAVEN	Risk Analysis Virtual Environment
SKI	Swedish Nuclear Power Inspectorate
SPH	Smoothed Particle Hydrodynamics
WISD	Wave Impact Simulation Device

Nuclear Power Plant Mechanical Component Flooding Fragility Experiments FY-2017 Report

1. INTRODUCTION

Nuclear Power Plant (NPP) mechanical component flooding fragility experiments and associated research has progressed throughout FY-2017. Progress includes execution of full scale fragility experiments using hollow-core doors, design, procurement, and installation of improvements to the Portal Evaluation Tank (PET), designation of experiments exploiting improved PET capabilities, component fragility mathematical model development, Smoothed Particle Hydrodynamic (SPH) simulations, coupling the SPH simulation code Neutrino with the INL Risk Analysis Virtual Environment (RAVEN) code, wave impact simulation device design, and pipe rupture mechanics research. Additionally, a component flooding steering committee charter was developed and initial committee membership was established.

Laboratory tours were conducted in February for INL representatives, in August for Idaho State Board of Education members, and also in August for the new Center for Advanced Energy Studies director. Presentations on the fragility experiment work were made to representatives of the Nuclear Regulatory Commission (February), Electric Power Research Institute (April), and the Korea Atomic Energy Research Institute (May). A presentation addressing progress on the flooding fragility work was made at the International Conference on Nuclear Engineering held in Shanghai, China July 2-6, 2017. The corresponding conference paper and presentation was selected as one of the five best North American student papers.

2. FULL-SCALE EXPERIMENTS

Full-scale experiments began with design and construction of the PET in 2016. The PET is a steel semi-cylindrical tank, with a height and diameter of 8 ft. It has a component testing window of 8 ft x 8 ft, two 3-in inlets on the sides, a 2-in outlet used for the draining system at the bottom, a new 12-in inlet, and four 1-1/4-in instrumentation ports were also added to the PET as part of the capabilities improvements performed in FY-2017.

The PET is connected through 3 in PVC pipe to a 5-HP submersible pump, located inside an ~8,000-gal water reservoir. An electromagnetic flow-meter continuously indicates the water flow into the tank, while an ultrasonic sensor and a pressure transducer are used to measure the water elevation within the PET and to calculate the leakage rate. The PET is also equipped with top mounted pressure and air relief valves and a pressure gauge; these instruments allow safe pressurized experiments in the PET. The initial PET piping configuration is shown in Figure 1.

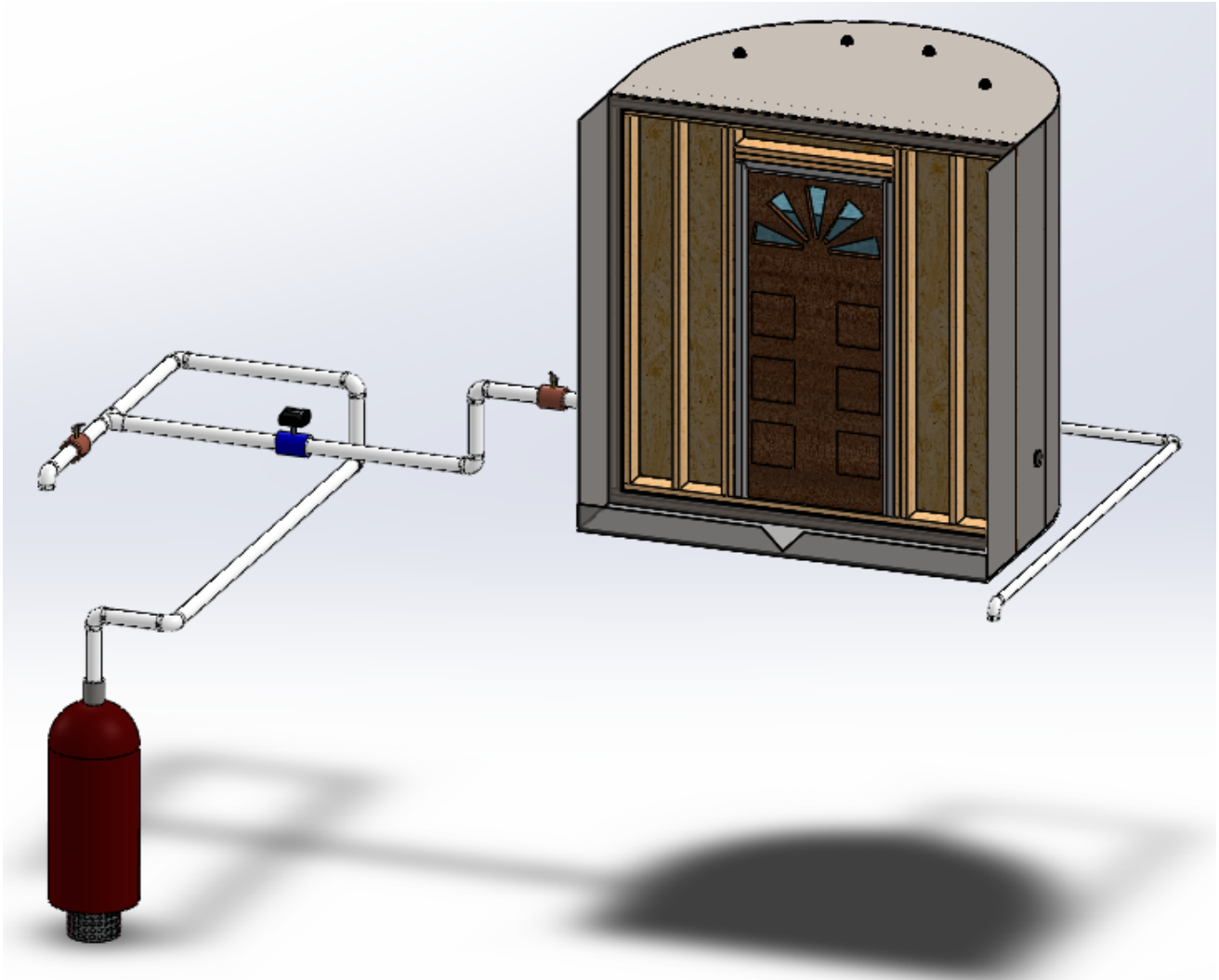


Figure 1. Initial PET piping configuration.

Five tests have been completed in the PET. All tests used hollow core doors, and involved water rise until catastrophic failure of the door occurred, or until the leakage rate equaled the pump flow rate capacity. The first three tests were conducted with the door opening outward, while in the latter two the door opened inward. The first test, Test 0, showed door bowing that resulted in equalization of leakage and input flow into the tank. See Figure 2 for a plot of depth versus time data.

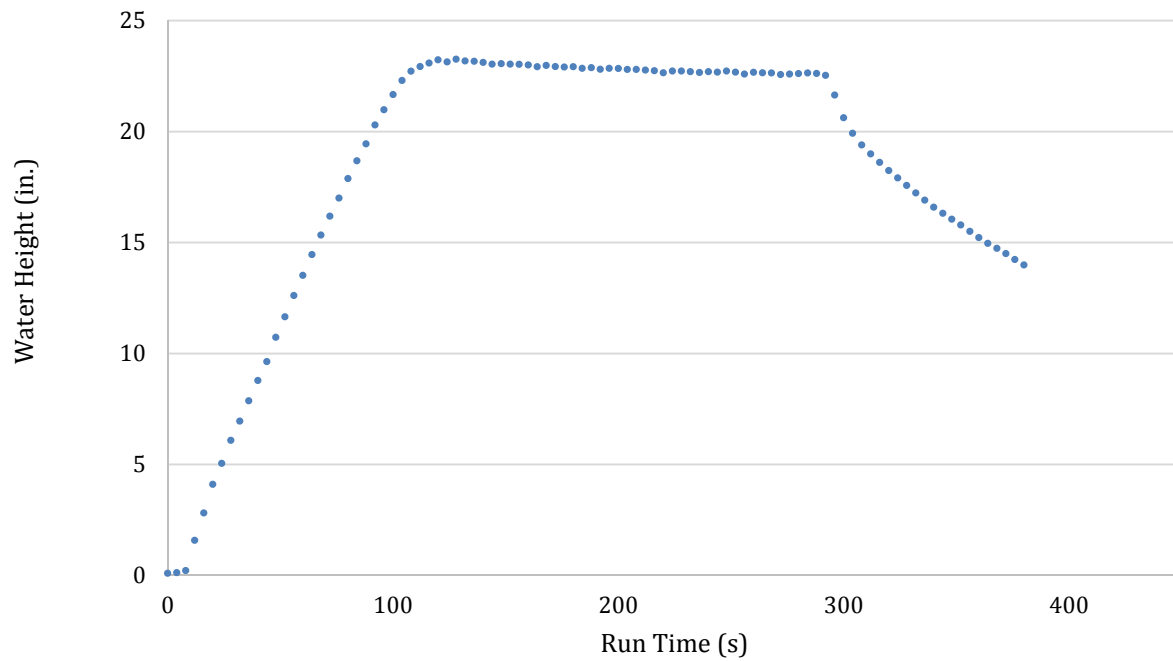


Figure 2. Water depth of test 0.

The bowing effect was reduced by attaching a 2.5-in wide plywood strip across the bottom of the door. This modification was used simply to determine if catastrophic door failure was possible. Two tests were performed with the plywood strip attached. Water depth versus time results of these tests (Test 1 and Test 2) are shown in

Figure 3. Both Test 1 and Test 2 resulted in catastrophic door failure, indicated by the rapid water depth reduction in the plot below, as the door failed and the water rapidly drained from the PET.

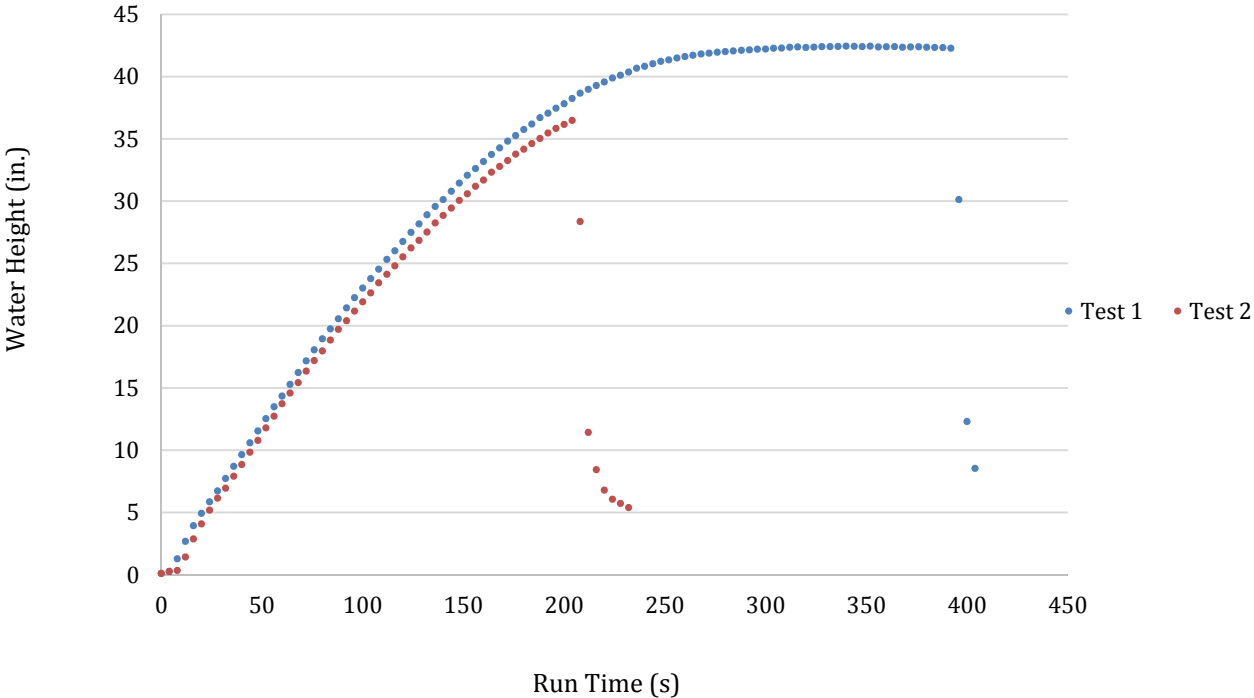


Figure 3. Water depth of tests 1 and 2.

Subsequent tests involved inward opening doors without the use of a plywood strip at the door bottom. As expected, a reduction in the water leakage rate occurred as the water inside the tank pressed the door against its frame. Catastrophic door failure occurred in both inward orientation tests at approximately the same water depth as the outward door orientation tests. Water depth versus time for Test 3 and 4 are shown in Figure 4.

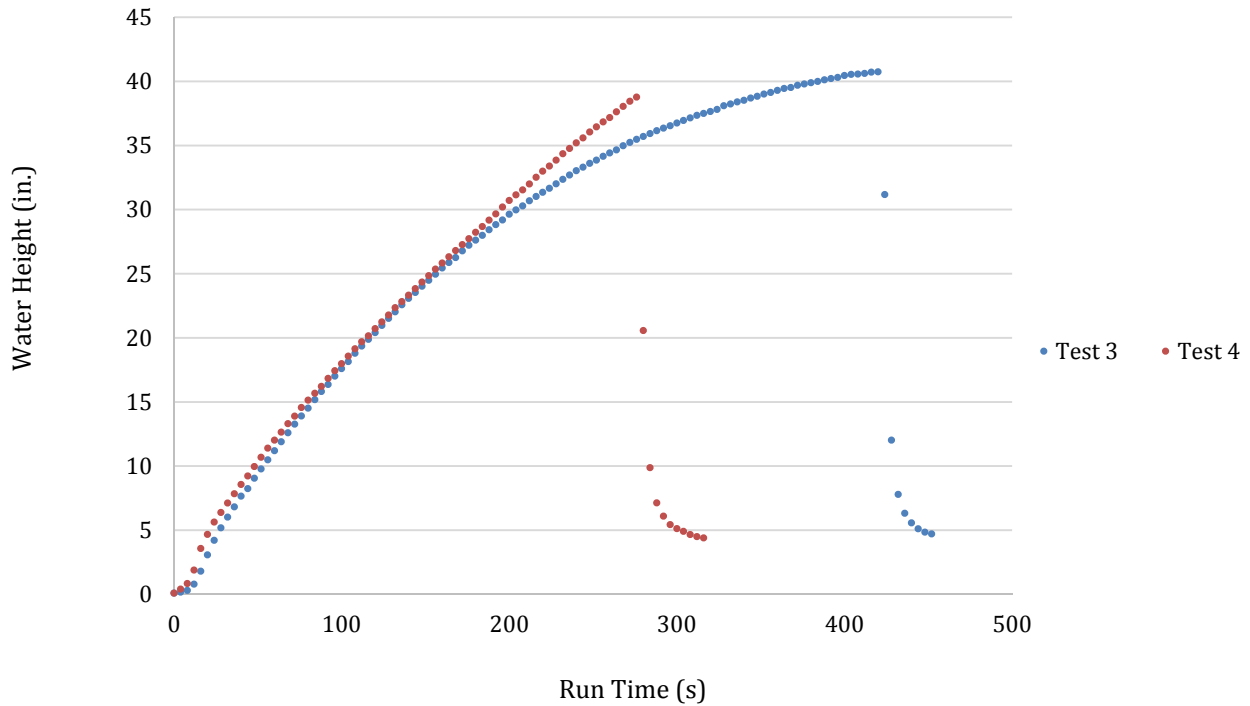


Figure 4. Water depth of tests 3 and 4.

These flooding fragility experiments involving simple hollow-core doors provided the opportunity to develop testing and data recording methodology. Data recorded from the tests were used to develop initial mathematical models for door fragility under flooding conditions. Additional discussion on the mathematical model development is provided below.

3. BAYESIAN REGRESSION FRAGILITY MODEL

Using the example Bayesian analysis model taken from reference [1], a flooding fragility model was developed using the door test data. For each of the experiments, data was collected for tank water depth (D), flow rate (F), and water temperature (T) as shown in Table 1. A failure (1) was assigned to tests where the damage to a door was permanent and the leakage area increased in a short amount of time. Success (0) is defined when an equilibrium state was reached between the flow rate and leakage rate.

Table 1. Door Test Data

Depth (in)	Flow Rate (gal/min)	Temp (F)	Failure
23.2	291.5	66	0
20.8	292.5	67	0
42.3	292.5	66	1
21.1	297.0	68	0
24.2	294.5	67	0
35.4	292.5	67	1
40.8	291.0	68	1
38.9	294.0	68	1

Applying a similar analogy of the example problem in reference [1], an assumption was made that depth, flow rate and temperature may be the parameters that affect the flooding fragility model in this case. The primary model was a binomial model with parameters p and $n=1$ (only one door is potentially challenged during testing). In this model, p is a possible function of depth, flow, and temperature. Following on the lines of the example problem, the parameter p is constrained between 0 and 1 and logit relation is used for p :

$$\text{logit}(p) = \ln\left(\frac{p}{1-p}\right)$$

The fragility model examined seven possibilities with each of the parameters alone driving the model to failure, a combination of two factors driving the model to failure, and a combination of all three factors driving the model to failure. These models are:

$$\text{logit}(p) = \text{intercept} + aD + bF + cT$$

$$\text{logit}(p) = \text{intercept} + aD$$

$$\text{logit}(p) = \text{intercept} + bF$$

$$\text{logit}(p) = \text{intercept} + cT$$

$$\text{logit}(p) = \text{intercept} + aD + bF$$

$$\text{logit}(p) = \text{intercept} + aD + cT$$

$$\text{logit}(p) = \text{intercept} + bF + cT$$

A script for OpenBUGS, a Bayesian analysis software tool using Markov Chain Monte Carlo (MCMC) methods, was written for the above seven equations. Since there was small variation in the flow rates and temperatures between runs, the outcome of failure is random with respects to these variables. Therefore, there is predictive capability on temperature and flow rate and the model had to be reduced to the depth variable when logit (p) function was used. This script is shown in Table 2.

Table 2. OpenBUGS Script for Depth Model

```
#Depth (D) Model
model {
for(i in 1:tests) {
    failure[i] ~ dbin(p[i], num.tested)
    # Regression model
    cloglog(p[i]) <- int + a*depth[i]
    #failure.rep[i] ~ dbin(p[i], num.tested) # Replicate values for model validation
    #diff.obs[i] <- pow(failure[i] - num.tested*p[i], 2)/(num.tested*p[i]*(1-p[i]))
    #diff.rep[i] <- pow(failure.rep[i] - num.tested*p[i], 2)/(num.tested*p[i]*(1-p[i]))
}
#chisq.obs <- sum(diff.obs[])
#chisq.rep <- sum(diff.rep[])
#p.value <- step(chisq.rep - chisq.obs)
# Prior distributions
int ~ dnorm(0, 0.0001)
a ~ dnorm(0, 0.001)
}
data
list(num.tested=1, tests=8, depth = c(23.23,20.75,42.3,21.05,24.22,35.41,40.76,38.85), failure =
c(0,0,1,0,0,1,1,1))
inits
list(int=0, a=0)
```

The results of running the script in Table 2 gives the depth coefficient and the intercept value as shown in Table 3. The Bayesian p-value was unavailable because the number of samples obtained was insufficient.

Table 3. Results of the Depth Model

Parameter	Mean Value
intercept	3.827
a (depth coefficient)	-110.2
Bayesian p-value	–

Since no conclusive result was obtained using the logit function, possible functions that could potentially replace logit were investigated. Once the necessary coefficient values are established, $\text{logit}(p) = \text{intercept} + aD + bF + cT$, would be re-modelled as:

$$p = \frac{1}{e^{-(\text{intercept} + aD + bF + cT)} + 1}$$

The shortcoming with the logit function was recognized and an attempt was made to check other available link functions that could provide complete results. The available link functions supported by OpenBUGS are log, logit, cloglog and probit [2]. They are defined as:

$\log(p)$: natural logarithm of p

$$\text{logit}(p) = \ln\left(\frac{p}{1-p}\right)$$

$\text{cloglog}(p)$: complementary log log of p $\ln(-\ln(1-p))$

$\text{probit}(p)$: inverse of standard normal cdf $\phi(p)$

Table 4 shows link functions behavior with designed flooding fragility models.

Table 4. Models Responses to Link Function

	Variables	log	logit	cloglog	probit
1	flow rate	•	✓	✓	❖
2	depth	•	✓	✓	❖
3	temperature	✓	✓	✓	❖
4	flow rate, depth	•	○	✓	❖
5	flow rate, temperature	•	✓	✓	❖
6	depth, temperature	•	○	✓	❖
7	flow rate, depth, temperature	•	○	✓	❖

The models with ✓ indicate complete results are available for intercept and coefficients. The symbols used in the table represent the errors returned and they are listed in Table 5.

Table 5. Errors Observed While Using Different Link Functions

Symbols	Observed Errors
•	Something went wrong in procedure; updater delayed. Sample in module updater.
○	Something went wrong in procedure. Sample in module update rejection.
❖	Something went wrong in procedure node. Value in module graph probit.

After testing the available link functions, only the cloglog script successfully ran for all seven models. Another way to predict the best model fit when the p-value is unavailable is using information criteria. This criterion measures the relative fit. A best model from the relative point of view may not be good from an absolute point of view. Two commonly discussed information criteria are the Bayesian Information Criteria (BIC) and Deviance Information Criteria (DIC). DIC is a measure of model fit that can be applied to Bayesian models and works when the parameter estimation is done using numerical techniques, such as Gibbs samplers. It is particularly useful in Bayesian model selection problems where the posterior distributions of the models have been obtained by MCMC simulation. DIC is a popular Bayesian analog of BIC. DIC has been recommended for selecting among the

hierarchical models. A hierarchical model, sometimes called multilevel model, has mutual dependence on the selected parameters that affect the modeling [3]. The door test data shows clear interdependence on the factors that have been selected to affect regression modeling.

In OpenBUGS, Dbar is automatically monitored by the node called *deviance*. It is the posterior mean of the deviance and it requires no additional scripting. Mathematically, DIC is calculated as the sum of Dbar and pD [4]:

$$\begin{aligned} \text{DIC} &= \text{Dbar} + \text{pD} \\ \text{pD} &= \text{Dbar} - \text{Dhat} \end{aligned}$$

Where, pD is the effective number of parameters and Dhat is the deviance evaluated at the posterior mean of parameter(s). DIC and even pD can be negative in some cases. DIC is usually negative when the density function is >1 . However, if pD is negative, DIC cannot be used. As a rule of thumb, the model with the smallest DIC indicates the best fitting model. For example, consider four models with DICs -11.5, -26, 10, and 56. The second model with DIC = -26 is the best fit model because it has the smallest DIC among the others. It must also be noted that since DIC is a measure of relative fit, a model with the smallest DIC can still be a poor fit.

The scripts were re-written to change the link function from logit to cloglog. First, the seven models were run for 100,000 samples. Next, DIC was selected from the inference menu of OpenBUGS. DIC was then set and the models were run for another 100,000 updates. The deviance information was then collected. Table 6 shows the results of the calculations.

Table 6. Information on DIC and Other Parameters of the Seven Models

Parameter	D, F, T	D	F	T	D, F	D, T	F, T
Intercept	5.653	-108.0	3.468	-6.659	3.289	-2.621	9.64
a (depth coeff)	42.37	3.72	–	–	43.14	36.23	–
b (flow rate coeff)	-7.109	–	-0.01354	–	-4.405	–	0.004231
c (temp coeff)	12.16	–	–	0.09177	–	-16.06	-0.1703
DIC	0.02266	0.2804	12.74	12.36	0.02729	0.03374	14.23

According to Table 6, the best fit model should be the first one (smallest DIC of 0.02266) which has all three parameters namely, depth, flow and temperature driving the model to failure.

To understand the shortcomings of the logit function, an attempt was made to determine whether increasing the variation of data values allowed the script to successfully run. This could affect the parameter range over which future experiments are conducted. Theoretical data was created with ten hypothetical tests, as shown in Table 7, using a combination of actual flow rates and depths along with values capable with the PET capability improvements under way.

Table 7 Hypothetical Door Test Data

Flow Rate (gal/min)	Depth (in)	Temperature (F)	Failure
146.4	16.56	65.98	0
152.5	22.46	67.04	0
149.8	18.97	66.02	0
292.5	38.85	67.67	1
291.0	40.76	66.60	1
297.0	21.05	66.87	0
294.5	42.30	68.33	1
1975.6	70.27	68.14	1
2861.3	84.43	66.86	1
2779.6	75.82	67.82	1

Applying the same seven fragility models with the logit function, the results of running the script with hypothetical data returned the error “Something went wrong in procedure Stack. Value in module GraphStack.” This error had previously been seen while trying to run sufficient samples to obtain the Bayesian p-value.

Upon further comparison with the analysis model taken from reference [1], it was noted that aside from the data being loaded, the only script difference was the binomial model parameter n. Only one door was challenged during testing (n=1), but the example had a demand put on six components (n=6) for each test. After changing n, the logit script successfully ran for any value of n greater than one with varying meaningless results.

Since the binomial model was not running when a single door was put on demand, other models were investigated. The selected model would still need to count failures, but also take a specified time period into account. The exponential distribution is a common aleatory model for time duration. If a system is running at time t, the probability that the system will fail in the next small-time interval Δt is $\lambda \Delta t$, for constant λ . This model interpretation corresponds with how door failure tests are conducted, and could return meaningful results. While the binomial model works for experiments with several components being tested at once (e.g. a wall of multiple feed-throughs), the model may change for each component type.

The path forward for the Bayesian analysis is to further investigate the exponential model and incorporate it along with time based data into an OpenBUGS script for door failure. Work with the logit function has influenced future experiment plans in that multiple parameter monitoring must involve some variation in the parameters during the test. The information from the hollow core door modeling will also help in future testing of different component types and consideration of other variables.

4. PET CAPABILITY IMPROVEMENTS

Following initial door testing experiments in the PET, design work was pursued to improve the PET capabilities. The initial PET door tests were limited to a single inlet flow rate of ~300 gpm. Additionally, the initial piping configuration did not allow tests where the tank was pressurized to simulate additional hydrostatic head. Limitations associated with data recording and video recording were also identified in the initial tests. Modifications to the PET were designed to support variable inlet flow rates up to ~4500 gpm. The designed modifications also support completely filling the PET and then relying on the pump to provide hydrostatic head to simulate water depths up to 20 ft. Additionally, design work was pursued to improve data and video recording.

The improved PET piping configuration is shown in Figure 5. The PET is connected to a 12 in piping network (Figure 6) linking the PET to an existing high displacement pump.

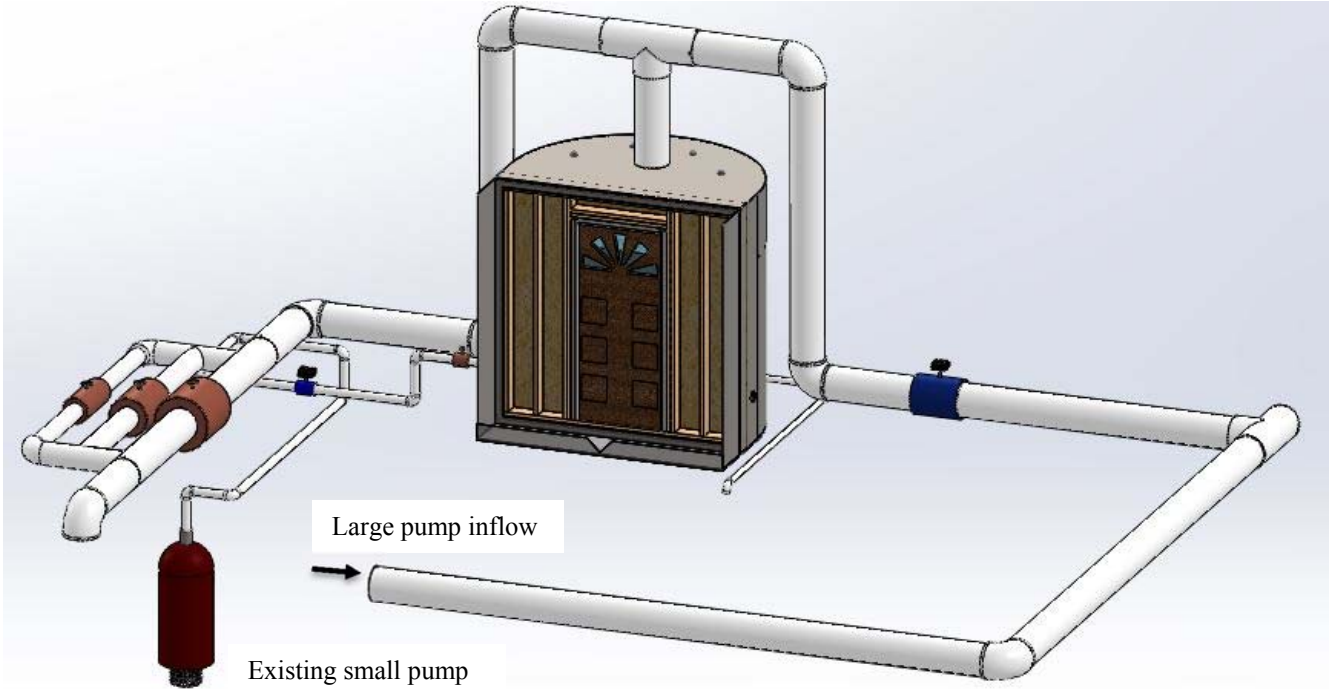


Figure 5. Improved PET piping configuration.



Figure 6. Existing 12-in pipe flanging with new piping installed.

The new piping installation work has proceeded over the course of the summer. The current configuration is visible in Figure 7. A new 12 in flange, see Figure 8, has been fitted at the top of the PET and is used to connect the PET to the new piping configuration. Within the PET, the 12 in pipe section extends down to the bottom of the PET, seen in Figure 9. Multiple holes are drilled in the PET piping section to improve the inlet flow distribution to the PET. The holes are positioned so that they do not face the opening wall directly, as the jets from them would affect tests. There are 38 2 in diameter holes drilled into the pipe giving an outlet area that is more than twice the area of the 12 in diameter inlet.



Figure 7. PET high flow piping.

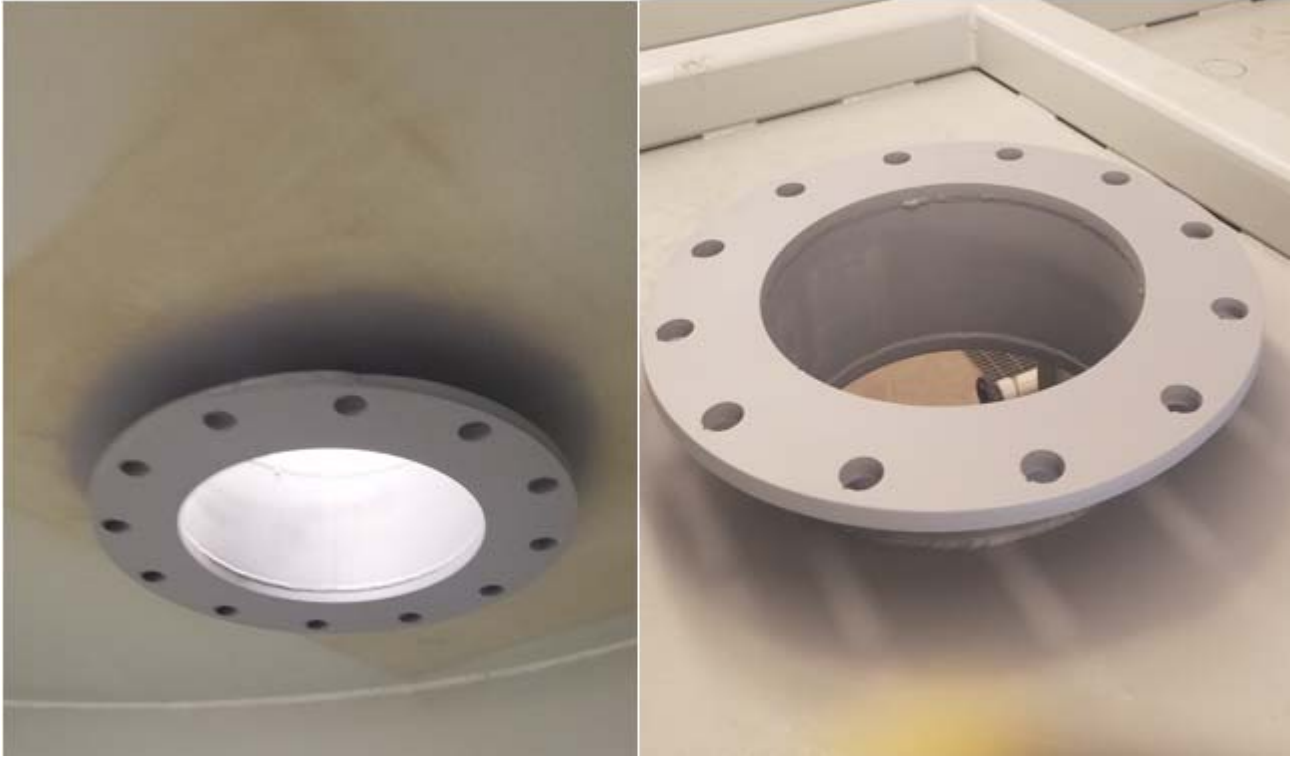


Figure 8. New PET pipe flange, inside (left) and outside (right).



Figure 9. PET stand pipe for 12-in line.

The new piping configuration contains a 12-in and an 8-in flowmeter and flow control valves in the downstream side of the PET. The flowmeters were delivered on September 1st and the piping upgrades are nearly complete. The flow control valves allow for large and small water flowrates through the downstream section of the piping system which in turn will control the flow rate into the PET. The new flow meters in conjunction with the flowmeters in the existing piping section, as seen in Figure 10, will be used to measure the flowrate entering the PET. The PET downstream piping bifurcations, flowmeters, and control valves are shown in Figure 11.

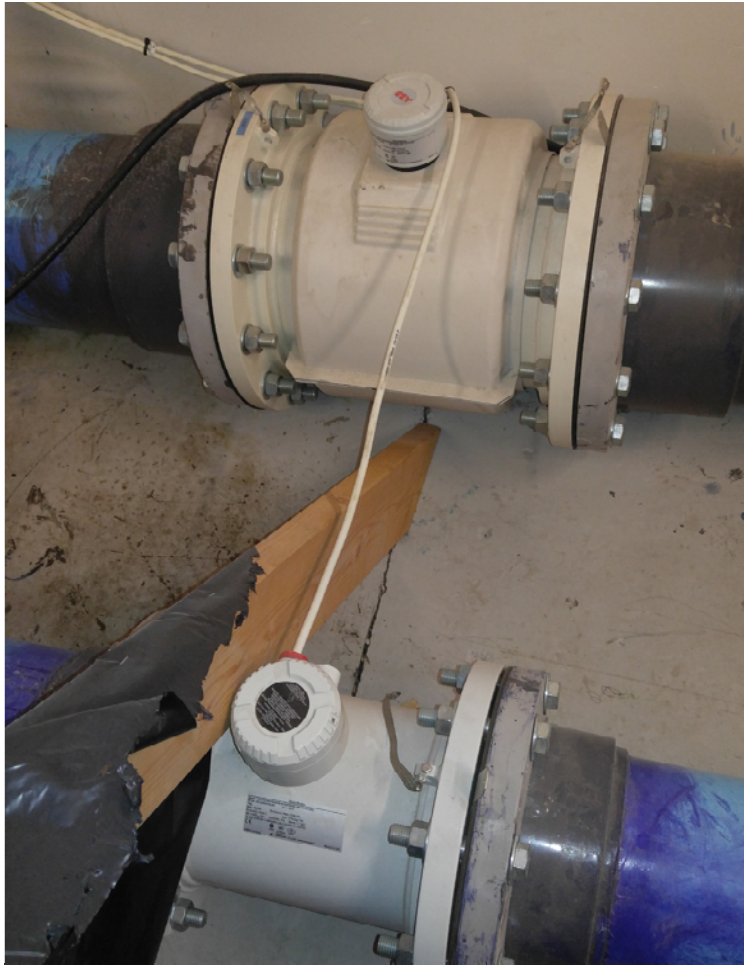


Figure 10. Existing 12 in flow meter (top) and 8 in flow meter (bottom).



Figure 11. PET downstream piping bifurcations, flow meters, and control valves.

The flow control area consists of 12 in, 8 in, and 6 in pipe sections in parallel each fitted with a gear actuated butterfly valve. This is the section downstream from the PET after the tee at the top of the tank. Closure of the valves will increase the total headloss in the system causing an increase of the water inlet flowrate into the PET, while opening of the valves will have the inverse effect. The piping system is also fitted with pressure relief valves to prevent possible air pockets.

A step-by-step guide has been prepared to safely perform pressurized tests. The guide includes the use of the downstream valves to reduce the inlet flow to the PET after a specific water depth has been reached. The reduced water flow will decrease the pressure spike that occurs once a system becomes completely filled with water. Once the PET has been filled with water, the downstream valves will continue to be operated until a 20 ft total head has been reached.

The last set of changes to the PET corresponds to the inclusion of a water inundation testing area downstream of the PET component wall. This was achieved by relocating the PET and the addition of splash guards. The splash guards will include clear acrylic sections to provide view points for cameras. Figure 12 shows the splash guards staged for installation.



Figure 12. Acrylic sheeting splash guard.

The PET also received two instrumentation upgrades. The first consists of additional data recording instrumentation, while the second consists of improved video recording cameras. The new data recording instrument consists of an OMEGA PX37-015GI water level sensor. This new sensor will be used as a validation tool for the data obtained by the currently used Campbell Scientific Instruments water level sensor, while also providing additional data sets for the water depth inside the PET. The new video recording cameras consist of four Sony FDRX3000 units. These are rugged action cameras that also provide high speed recording capabilities and have the benefit of already coming with waterproof housings. One of the cameras will be placed inside the PET, while the other three will be placed at different points outside the PET.

The remaining PET upgrades include integration of the new instrumentation, sealing the tank's instrumentation ports, and welding support straps for the new piping.

Lastly, work is being pursued related to pipe rupture tests. These tests will use the 300 gpm pump from the previous PET experiments. These experiments are proceeding in the planning stages. These tests will focus on leakage from pipes 3 inches in diameter or less, as these have been found to be some of the most common pipe sizes to fail in nuclear power plants. These experiments will be done to determine the spray pattern from common pipe breaks and leaks at different flowrates and pressures. These results will then be used to build a database that can be used for risk assessment projects.

5. TESTING PLANS

With the PET capability improvements in place, a series of tests will be performed to confirm the new PET operating characteristics. These tests will use hollow-core doors with an inward opening configuration. The initial tests will focus on measuring flow and leakage rates. These tests will also exercise the new data and video recording equipment. Multiple hollow-core doors will be tested to the point of catastrophic failure. It is expected the data associated with these tests can be combined with the prior door tests. The addition of tests involving different flow rates will be used better inform the fragility model development.

Following confirmation of PET operating characteristics, a metal door will be installed in the PET and a series of fragility experiments will be performed. These tests will involve variation of flow rates and measurement of leakage rates. The initial metal door tests will restrict water depths to the height of the door. Catastrophic failure of a metal door is not expected when the water depth is restricted to the door height.

The metal door tests will then progress to pressurized PET tests. These tests will involve a methodical process where the hydrostatic head is incrementally increased. Multiple tests will be performed with the goal of achieving a hydrostatic head of 20 ft. Catastrophic failure of the door under a pressurized test is possible. Significant safety precautions will be instituted to ensure no personnel are injured in the event of catastrophic metal door failure.

Installation of utility feedthroughs in the wall supporting the door will also be pursued. The primary intent of these additions is measurement of leakage rates. Feedthrough tests with and without a fire barrier will be performed.

6. STEERING COMMITTEE CHARTER

To help guide the selection of components for testing as well as other aspects of the component fragility testing protocol, a steering committee charter has been developed. The charter is shown in Figure 13. Initial committee member invitations have been issued with some acceptances received (shown) and others pending. Additional invitations are also pending.

Idaho State UNIVERSITY

College of Science and Engineering
921 South 8th Avenue, Stop 8065 - Pocatello, Idaho 83209-8065

Component Flooding Evaluation Laboratory Steering Committee Charter August 17, 2017

Purpose

The Component Flooding Evaluation Laboratory (CFEL) Steering Committee (CSC) provides technical review, strategic guidance, and oversight concurrence for component based flooding fragility experiment priorities and protocol, associated mathematical model application, and flooding simulation development strategies.

Scope

1. The CSC shall provide technical review of all proposed component flooding fragility experiments, fragility mathematical model approaches, and flooding simulation techniques.
2. The CSC technical review shall consider nuclear power industry impacts, nuclear power regulatory impacts, risk analysis strategy impacts, overall programmatic cost impacts, and proposed experiment safety implications.
3. The CSC shall provide strategic guidance for potential component flooding fragility experiments, fragility mathematical model and flooding simulation development strategies.
4. The CSC strategic guidance shall consider CSC member experience, nuclear power industry impacts, nuclear power regulatory impacts, risk analysis strategy impacts, and overall programmatic cost impacts.
5. The CSC shall periodically review results of component flooding fragility experiments.

Reporting, Membership, and Protocol

1. The CSC reports to the ISU Flooding Experiments Director (Dr. Chad Pope).
2. The CSC chair shall be a member of academia.
3. The CSC membership shall include at least one member representing nuclear power industry interests.
4. The CSC membership shall include at least one member representing risk assessment research interests.
5. The Department of Energy RISMCM Pathway Lead shall be an *ex-officio* member of the CSC.
6. CSC membership shall be proposed by the CSC chair with concurrence by the RISMCM Pathway Lead.
7. CSC meetings may be conducted in person or via electronic methods.
8. The CSC Chair shall confirm a quorum is present for each meeting where a quorum consists of at least two-thirds majority of committee members.
9. CSC concurrence requires at least two-thirds of the CSC membership and must include the CSC Chair.
10. In cases where unanimous CSC concurrence is not achieved, dissenting opinions must be provided to the RISMCM Lead.

Members

Dr. Chad Pope, Idaho State University	Chair
Dr. Curtis Smith, Idaho National Laboratory	RISMCM Pathway Lead
Mr. Alan Moldenhauer, Dominion Energy	Member
Mr. Bently Harwood, Idaho National Laboratory (acceptance pending)	Member
Mr. Kelly Boodry, retired (acceptance pending)	Member

Phone: (208) 282-3099 • Fax: (208) 282-4464 • www.isu.edu
ISU is an Equal Opportunity Employer

Figure 13. Component Flooding Evaluation Steering Committee Charter.

7. SMOOTHED PARTICLE HYDRODYNAMICS

Smoothed Particle Hydrodynamics (SPH) is a method for modeling fluid flow and is being investigated for flooding event simulation. The goal is to be able to either incorporate flooding failure data obtained from CFEL into an SPH code or to couple an SPH code with a risk assessment code that has the flooding failure data. Incorporating SPH and flooding failure data would allow for flooding simulations at NPPs to be modeled before a flooding event occurs. This would allow the NPP to determine what damage would be done if the simulated flooding event was to occur. Additionally, it would also help determine if certain actions need to be taken that would reduce the damage of the flooding event. For example, if a 15-m tsunami at the Fukushima Daiichi plant could have been simulated, the simulation might have showed the backup generators were going to be impacted and possibly fail. Therefore, the plant could have relocated the generators which may have reduced the devastation of the accident.

For flooding scenarios to be adequately modeled, SPH codes need to be compared to physical results to determine the reliability of the code. Therefore, two items are needed to execute a comparison between physical results and an SPH model: a physical experiment with results and an SPH code. The physical experiment used here is flow over an ogee spillway and the SPH code used is the developmental code Neutrino.

The physical experiment used for this comparison was conducted using a scaled model of an ogee spillway with a horizontal apron [5] [6]. The scaled model experiment was conducted at the Utah Water Research Laboratory in Logan, Utah. The spillway was constructed of Plexiglas so that smooth curves could be obtained and pressure taps could be easily installed along the spillway. The ogee spillway was approximately 0.80 m tall, 1.83 m wide, and 1.36 m long and was placed in a flume with approximate dimensions of 12 m long, 1.83 m wide, and 1.22 m high.

The experiment consisted of setting different values of the upstream head, measured approximately 2 m upstream, and then taking flow rate and pressure measurements. The flow rate measurements were taken using weight tanks, volumetric tanks, or an ultrasonic flowmeter. Several measurement tools were used because each device measured different flow rate quantities. The weight tanks were used at low flow rates, the volumetric tanks were used for the intermediate to high flow rates, and the ultrasonic flowmeter was used at the two highest flow rates.

Once the experiment for the scaled model was completed and the results recorded, the results were then scaled up 30 times to prototype scale. One difference between the scaled model and the prototype is that the prototype has a silt level behind the spillway. The silt level is essentially the ground level behind the spillway after fine sand and clay has built up. The prototype scale is what was used for the SPH comparison since that scale represents an actual spillway.

Neutrino is a general-purpose simulation and visualization environment developed by Neutrino Dynamics Initiative which includes an SPH solver [7]. Neutrino is being used for a variety of applications including risk assessment and mitigation, hydro-fracturing, energy research, and environmental sciences [7]. Neutrino is a proprietary, developmental code but is available to universities for research. The Neutrino version used for this comparison was Neutrino_Windows_vc12_2016_08_29 which contains a known leakage issue resolved by placing rigid bodies in the area of leakage.

The Neutrino model was comprised of the following components: a rigid custom (spillway), a rigid box (flume), 9 rigid cuboids (1 for silt level, 8 for leakage), the IISPH fluid solver, 2 square particle emitters to fill the area behind the spillway, 1 flow particle emitter to set the flow rate, 1 measurement field to measure the total head

60 m upstream, and 2 particle killers to remove particles at the end of the spillway and any particles that might leak from the system. Figure 14 shows the Neutrino model with the spillway.

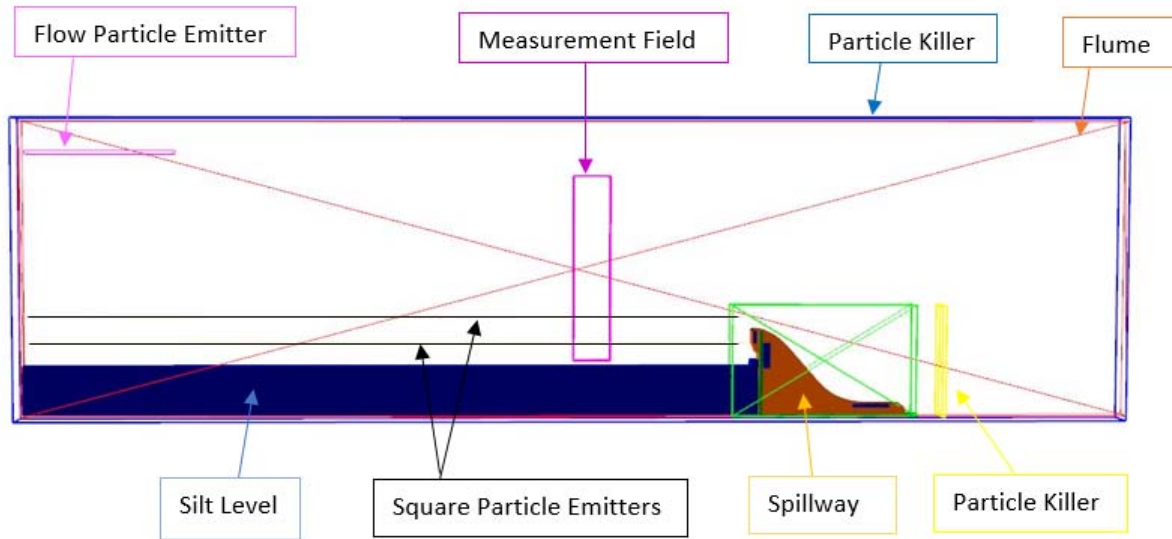


Figure 14. Neutrino model configuration.

The fluid and rigid body properties used default values based on the Neutrino developer’s advice except for kinematic viscosity which was set to $1.4 \times 10^{-6} \text{ m}^2/\text{s}$ which is the kinematic viscosity at the water temperature of the physical model.

Two parametric studies were performed to determine certain properties of the model. The two parametric studies were on the width of the model and the particle diameter of the fluid. The goal of these parametric studies was to determine the most computationally efficient model. The first parametric study was on the width of the system. This was done because the spillway model is essentially a 2D model. The properties and measurements do not change as a function of width. However, since the Neutrino model includes a flume, the width of the model cannot be so small that sidewall affects are occurring where the measurement is being taken.

The width parametric study was conducted by decreasing the width of the entire Neutrino model, running the model, and then measuring the water surface elevation. The calculations were performed on a computer with 32 GB RAM, 1 TB Hard drive, 15 TB External storage, 2 NVidia GeForce GTX Titan X 12 GB graphics cards, and a 3.00 GHz Intel® Core™ i7-5960X CPU. The water surface elevation was measured to make sure that sidewall affects were not occurring. The particle diameter that was used for this parametric study was 0.5 m which was the default Neutrino value and the flow rates used were $1.90 \text{ m}^3/\text{s}/\text{m}$, the lowest flow rate of the ten runs, and $89.9 \text{ m}^3/\text{s}/\text{m}$, the highest. Table 8 shows the width parametric study results, Figure 15 shows the plot of the water elevation vs. time for the different model widths at the low flow rate, and Figure 16 shows the plot of water elevation vs. time for the different model widths at the high flow rate. The fluctuations at the beginning of the plots are from filling the area behind the spillway with particles.

Table 8. Width Parametric Study Results

Model Width (m)	Flow Rate (m ³ /s/m)	Simulation Time for 15,000 Time Steps (hours)
7	1.90	14.08
7	89.90	28.03
6	1.90	12.52
6	89.90	24.63
5	1.90	10.19
5	89.90	18.99
4	1.90	8.04
4	89.90	16.32
3	1.90	6.10
3	89.90	12.37
2	1.90	3.73
2	89.90	8.24

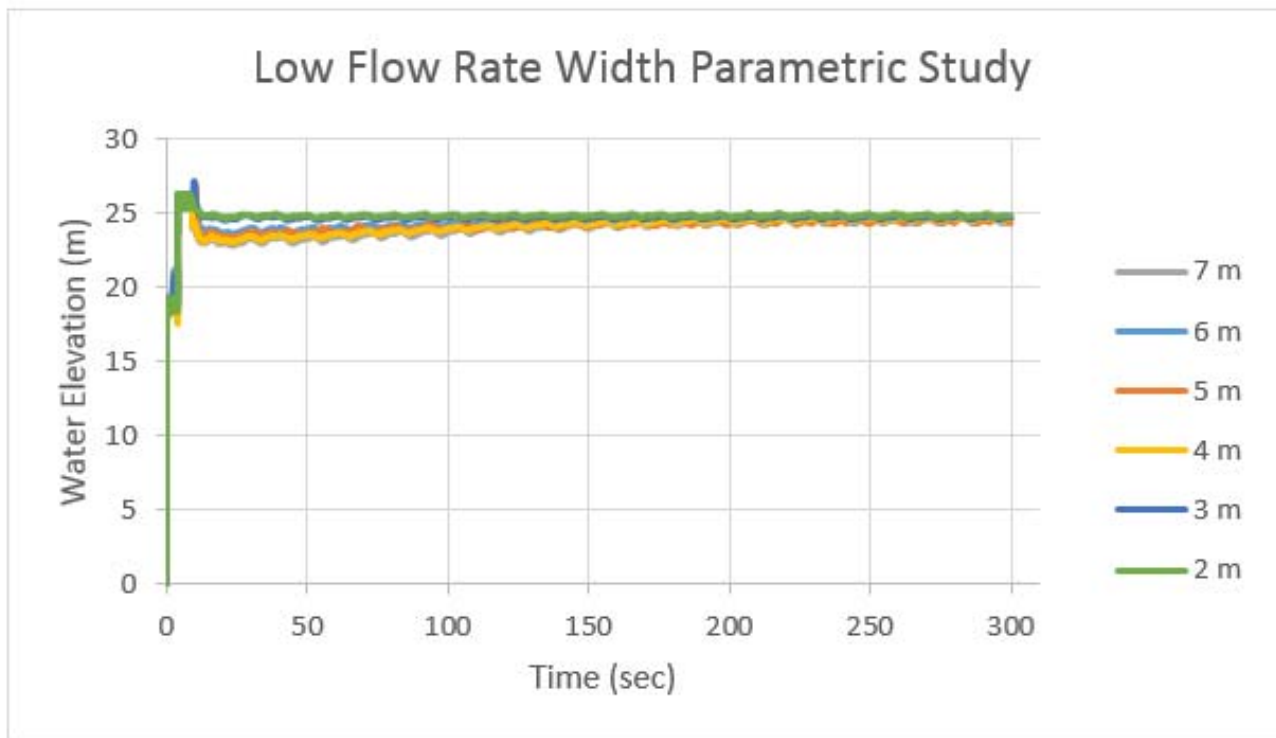


Figure 15. Low flow rate width parametric study plot.

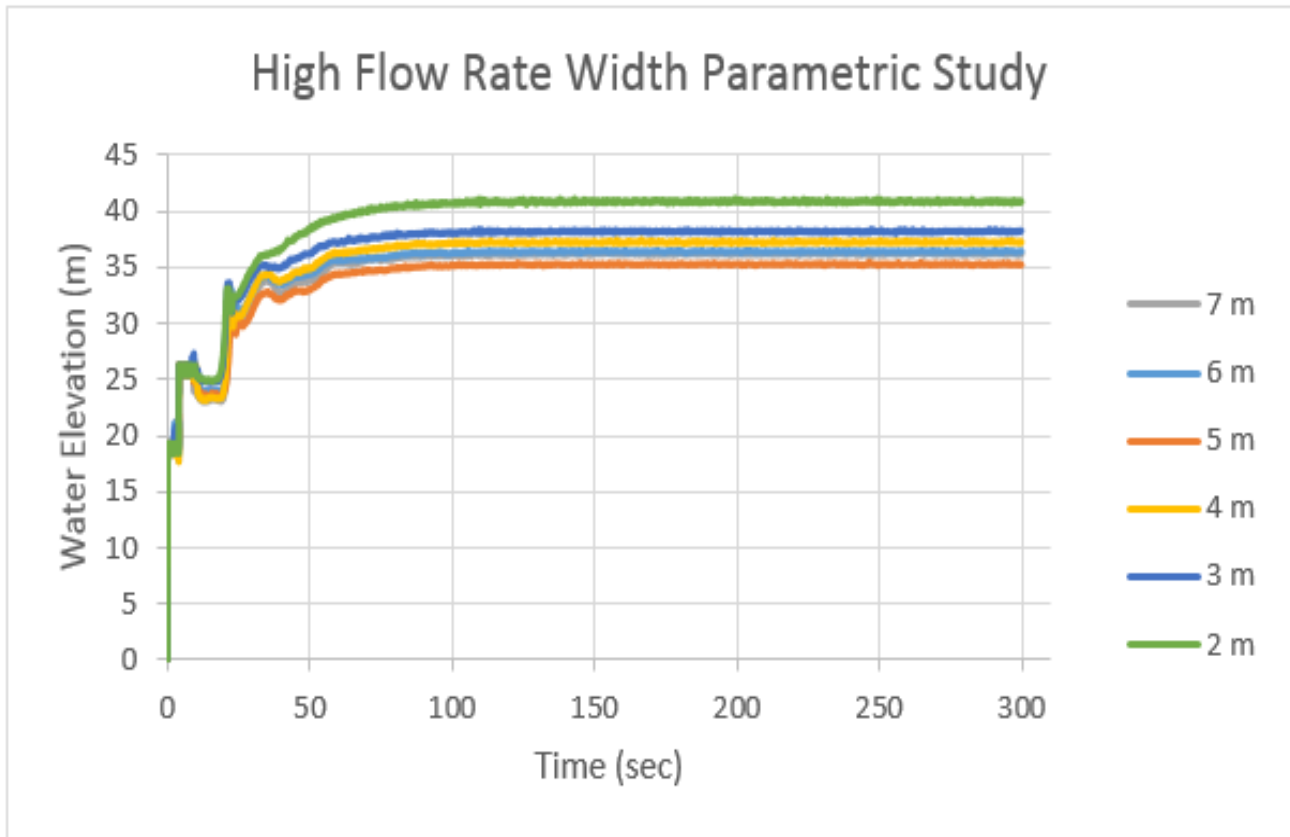


Figure 16. High flow rate width parametric study plot.

From the above results, the low flow rate water elevation does not seem to change much as the model width is decreased except for the 2-m model width. However, there is fluctuation in water elevation for the high flow rate as the model width was adjusted. Based on the high flow rate plot, the 7-m model width and 6-m model width provided almost identical results. The model widths of 3 m, 4 m, and 5 m are grouped around the 6-m and 7-m model widths. The 2-m model width result is above the rest of the results showing that sidewall effects are occurring. Therefore, a model width of 4 m was determined to be used for this comparison. The 4-m model width was chosen because it provided results that were close to the 7-m model width and reduced the simulation time by over 40%.

The second parametric study focused on particle diameter. This was done to determine the largest sized particle that can be used such that making the particle any smaller will not change the result. The parametric study was conducted by decreasing the diameter of the fluid particles, running the model, and then measuring the water surface elevation. The water surface elevation was measured to determine how different particle diameters would affect the results. Table 9 shows the particle diameter parametric study results, Figure 17 shows the plot of water elevation vs. time for the different particle diameters at the low flow rate, and Figure 18 shows the plot of water elevation vs. time for the different particle diameters at the high flow rate. Again, the fluctuations at the beginning of the plots were from filling the area behind the spillway with particles.

Table 9. Particle Diameter Parametric Study Results

Particle Diameter (m)	Flow Rate (m ³ /s/m)	Simulation Time for 15,000 Time Steps (hours)
0.5	1.90	8.03
0.5	89.90	16.32
0.45	1.90	10.76
0.45	89.90	22.27
0.4	1.90	14.92
0.4	89.90	31.63
0.35	1.90	19.09
0.35	89.90	46.47
0.3	1.90	28.75
0.3*	89.90*	64.96*

* This run was simulated for only 260 seconds due to storage limitations

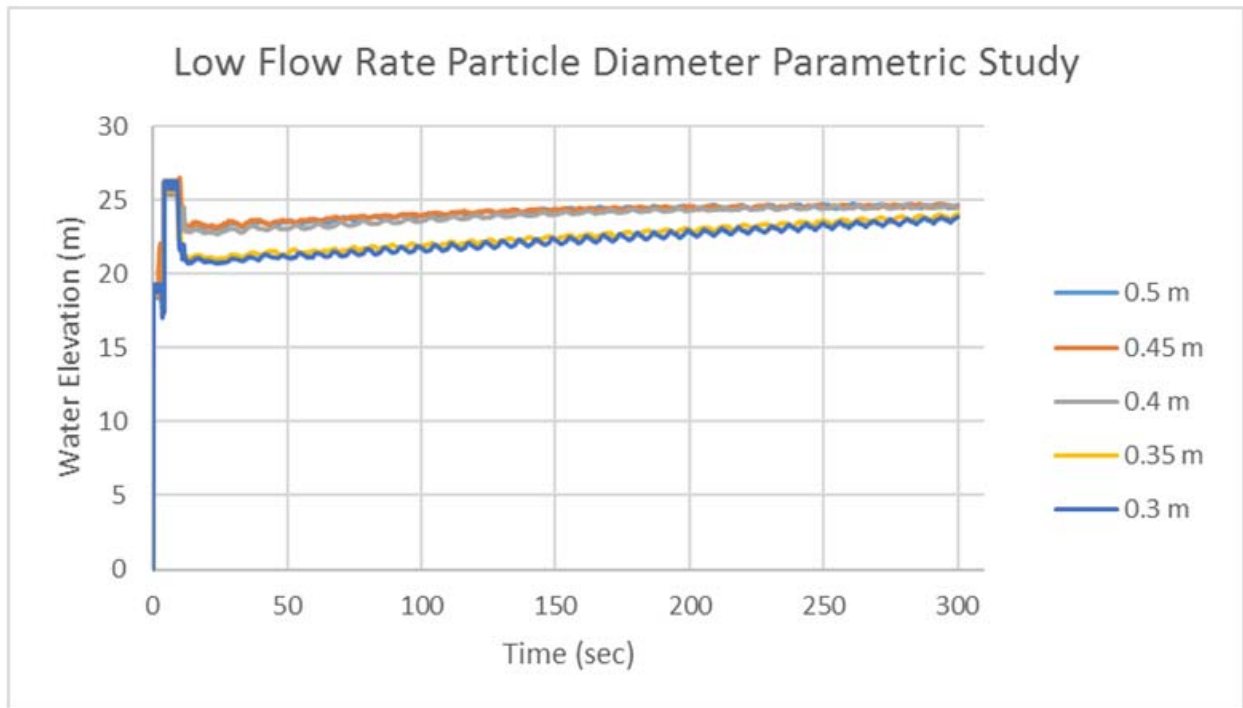


Figure 17. Low flow rate particle diameter parametric study plot.

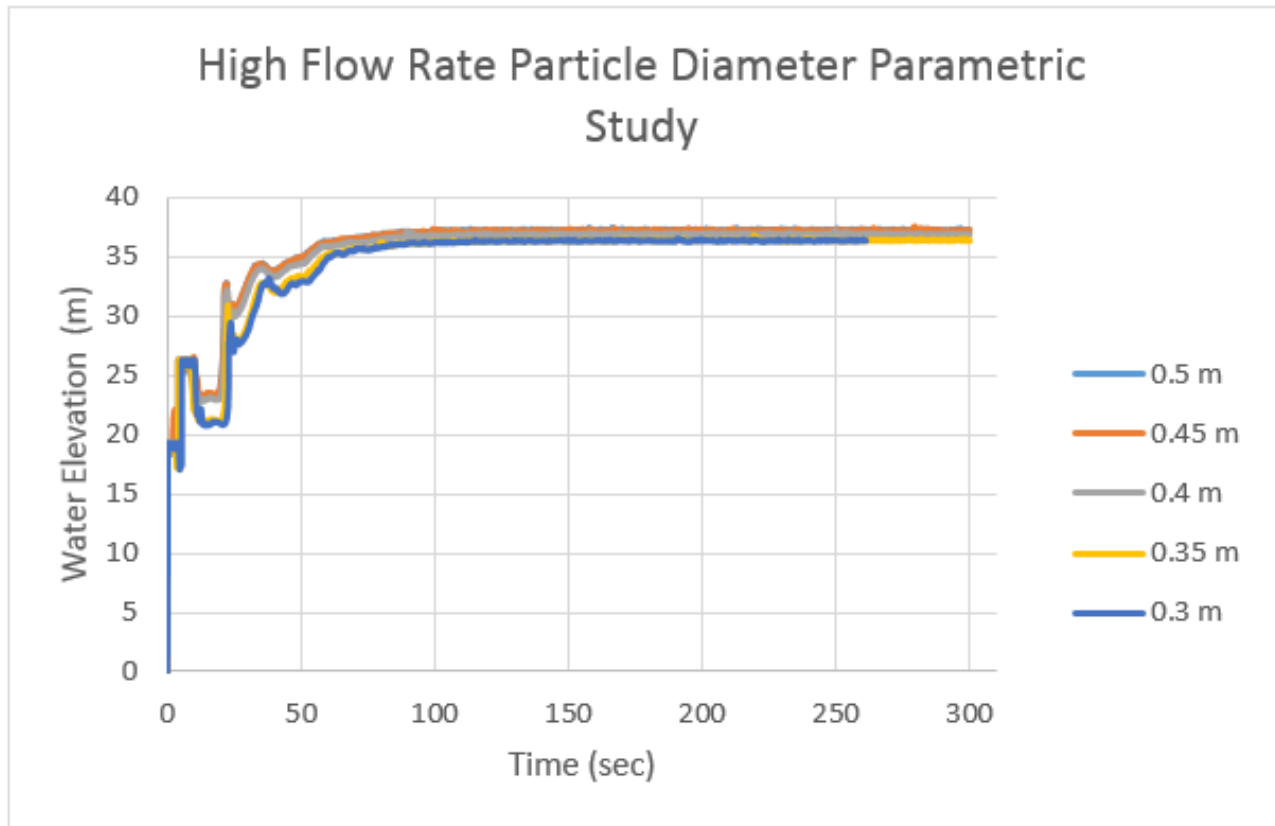


Figure 18. High flow rate particle diameter parametric study plot.

From the above results, the water elevation results decrease as the particle diameter decreases for both the low and high flow rates. For both flow rates, the 0.5-m, 0.45-m, and 0.4-m particle diameters were all grouped together and the 0.35-m and 0.3-m particle diameters were grouped together. Since smaller particles provide better results, the 0.35-m or 0.3-m particle diameter are a better choice. However, the goal was to have a computationally efficient model so the 0.35 m particle diameter was selected since it provided essentially the same result as the 0.3-m particle diameter, but reduced the simulation time.

To make sure the model width of 4 m was still reasonable, the model widths of 5 m and 3 m were rerun using the particle diameter of 0.35 m. Table 10 shows the results of the width parametric study with the new particle size, Figure 19 shows the plot of water elevation vs. time for the different model widths at the low flow rate, and Figure 20 shows the plot of water elevation vs. time for the different model widths at the high flow rate.

Table 10. Model Width Check Results

Model Width (m)	Flow Rate (m ³ /s/m)	Simulation Time for 15,000 Time Steps (hours)	Output Storage Space (TB)
3	1.90	14.44	0.90
3	89.90	35.73	2.32
4	1.90	19.09	1.14
4	89.90	46.47	2.97
5	1.90	24.99	1.55
5	89.90	57.31	3.75

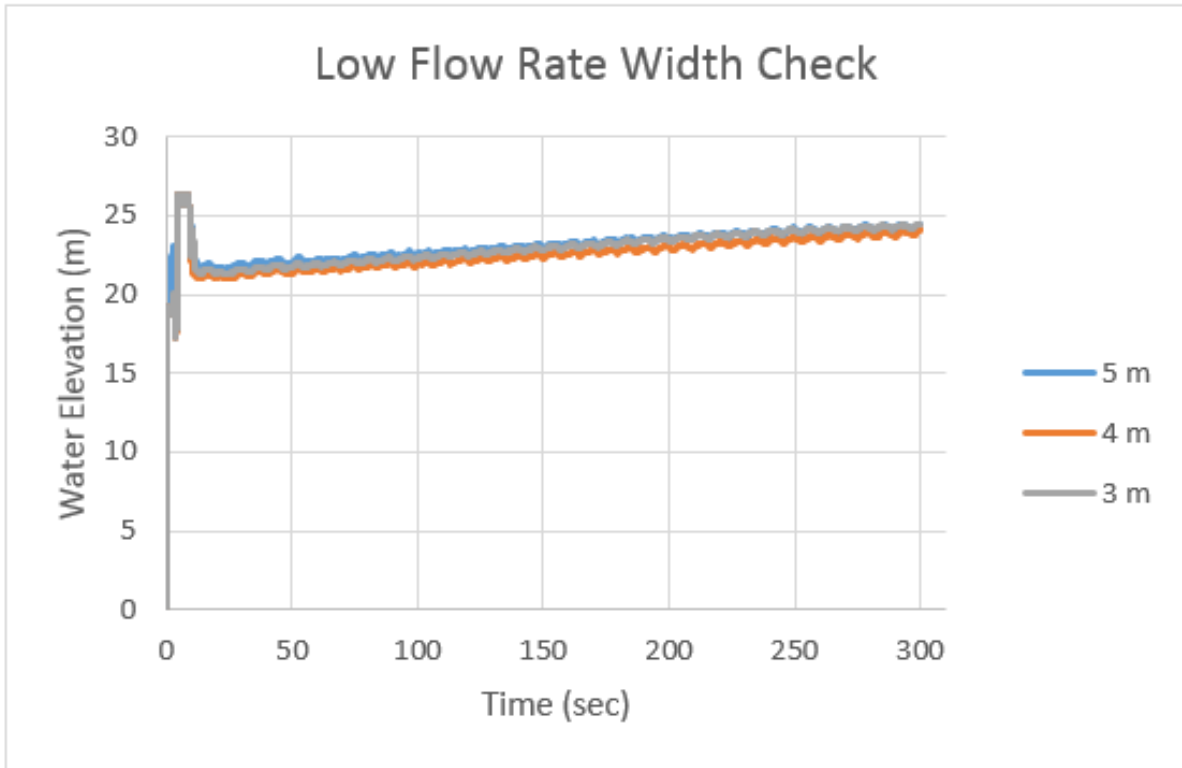


Figure 19. Low flow rate model width check plot.

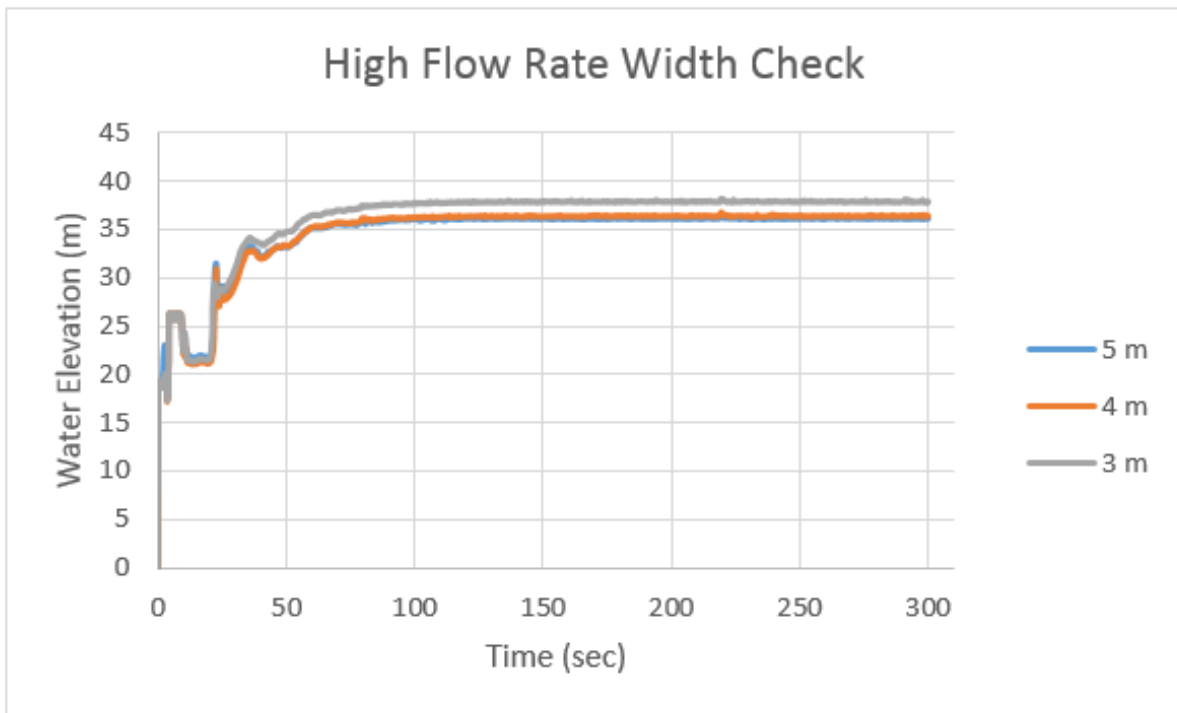


Figure 20. High flow rate model width check plot.

From the above results, the 4-m model width was determined to be wide enough such that sidewall effects would not occur. Based on the parametric studies, the final model width was 4 m and the final particle diameter was 0.35 m.

The parametric studies show the particle diameter and geometry simplification are both functions of flow rate and more research needs to be conducted to determine a method or guidelines for selecting the appropriate particle diameter and geometry simplifications. While the particle diameter and geometry simplification were investigated for model optimization, there are other parameters that could possibly effect the results as well. These parameters could be density, fluid viscosity, or friction factors, but these parameters were not studied to determine their effect on the results and is left for future research.

For the ten runs, each run was simulated for 15,000 frames where each frame is 0.02 seconds of real time. Therefore, 5 minutes of real time for each run was simulated. The measurements were taken during the last 1,500 frames, or for the last 30 seconds of the simulation. This was done so that there would be enough data points to get a good average for the measurement and because steady state had been reached by that time frame. The steady state was determined by plotting the standard deviation of the water elevation as a function of time. This was done for the lowest and the highest flow rate. Figure 21 shows the water elevation vs. time plot for the lowest and the highest flow rate and Figure 22 shows the water elevation standard deviation vs. time plot for the lowest and highest flow rate. The standard deviation plots start half way through the simulation (at 150 seconds) since the area behind the spillway was filling up at the beginning of the simulation.

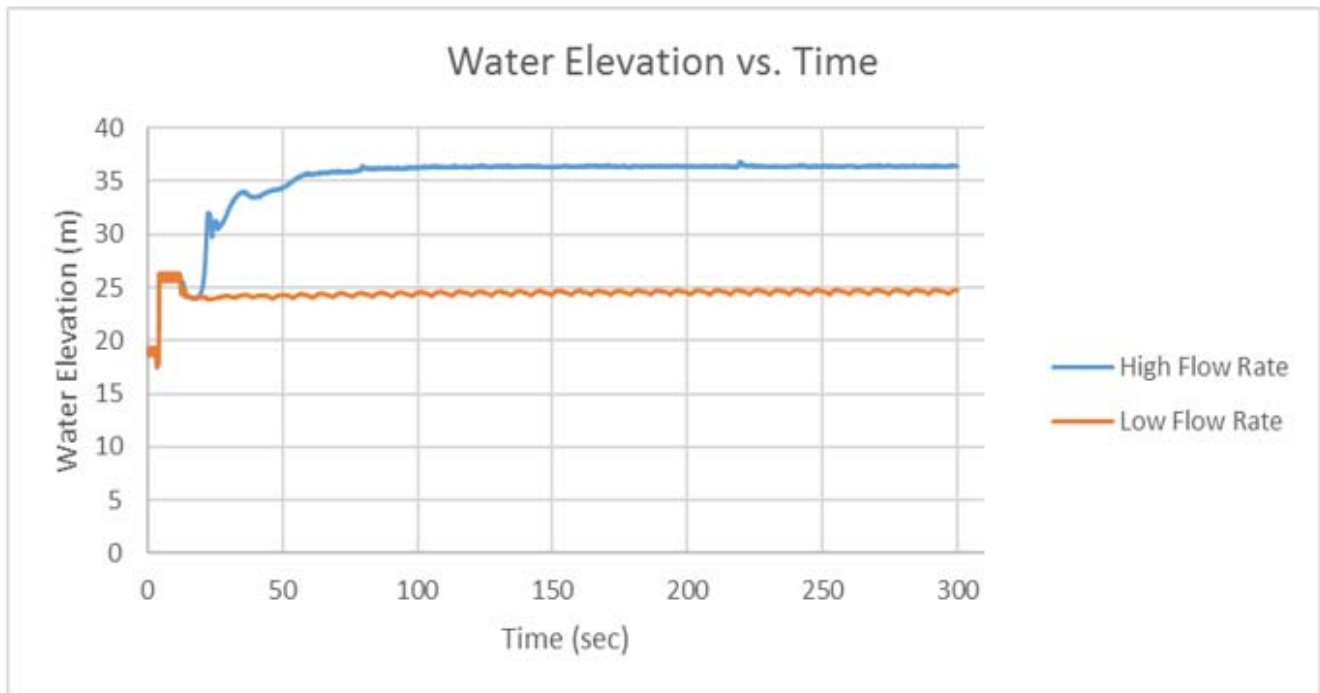


Figure 21. Water elevation vs. time plot.

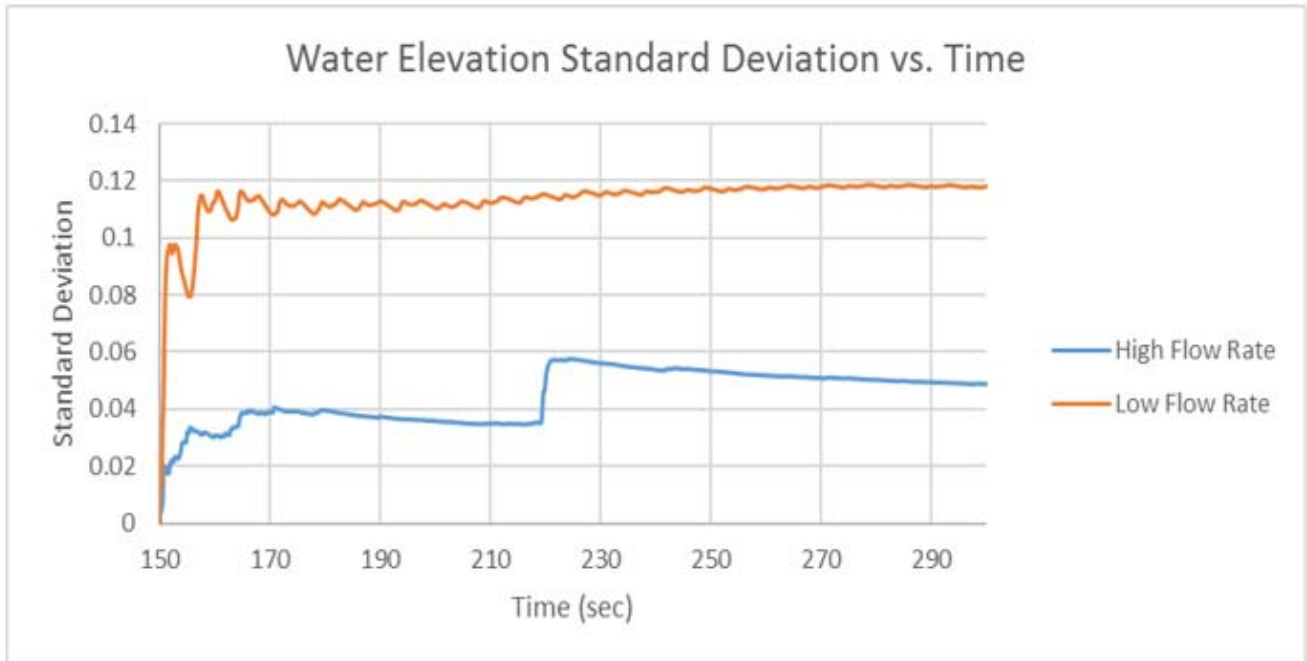


Figure 22. Water elevation standard deviation vs. time plot.

Based on the plots above, the steady state section was determined to have occurred since both plots had essentially leveled out by the time measurements were taken. The high flow rate standard deviation plot had a jump due to a rise in the water elevation at about 220 seconds. However, any slight change in water elevation will cause a jump in the standard deviation since the standard deviation is small.

The results for the comparison are shown below. Table 11 shows the details of each of the ten runs, Table 12 shows the physical results, SPH results, and relative percent error between the two for each run, Figure 23 shows the plot of total head vs. flow rate for both the physical and SPH results, and Figure 24 shows the plot of total head relative percent errors between the SPH and physical results.

Table 11. SPH Result Details

Run	Simulation Time (hours)	Number of Particles at Last Time Step	Storage Space (TB)
1	22.38	191,730	1.39
2	24.31	215,560	1.54
3	27.16	241,336	1.71
4	28.68	263,999	1.86
5	31.84	289,861	2.04
6	34.06	314,291	2.21
7	36.70	340,717	2.39
8	38.96	364,808	2.56
9	42.21	397,493	2.79
10	46.57	432,263	3.02

Table 12. SPH and physical results for total head and flow rate comparison

Run	Flow Rate (m ³ /s/m)	Physical Total Head Result (m)	SPH Total Head Result (m)	Relative Error (%)
1	1.90	24.27	24.62	1.45
2	6.03	25.33	25.86	2.09
3	12.29	26.48	27.28	3.00
4	19.02	27.37	28.40	3.78
5	27.92	28.47	29.83	4.79
6	37.79	29.50	31.11	5.45
7	48.24	30.44	32.50	6.75
8	58.86	31.35	33.83	7.90
9	73.77	32.42	35.56	9.70
10	89.90	33.45	37.38	11.74

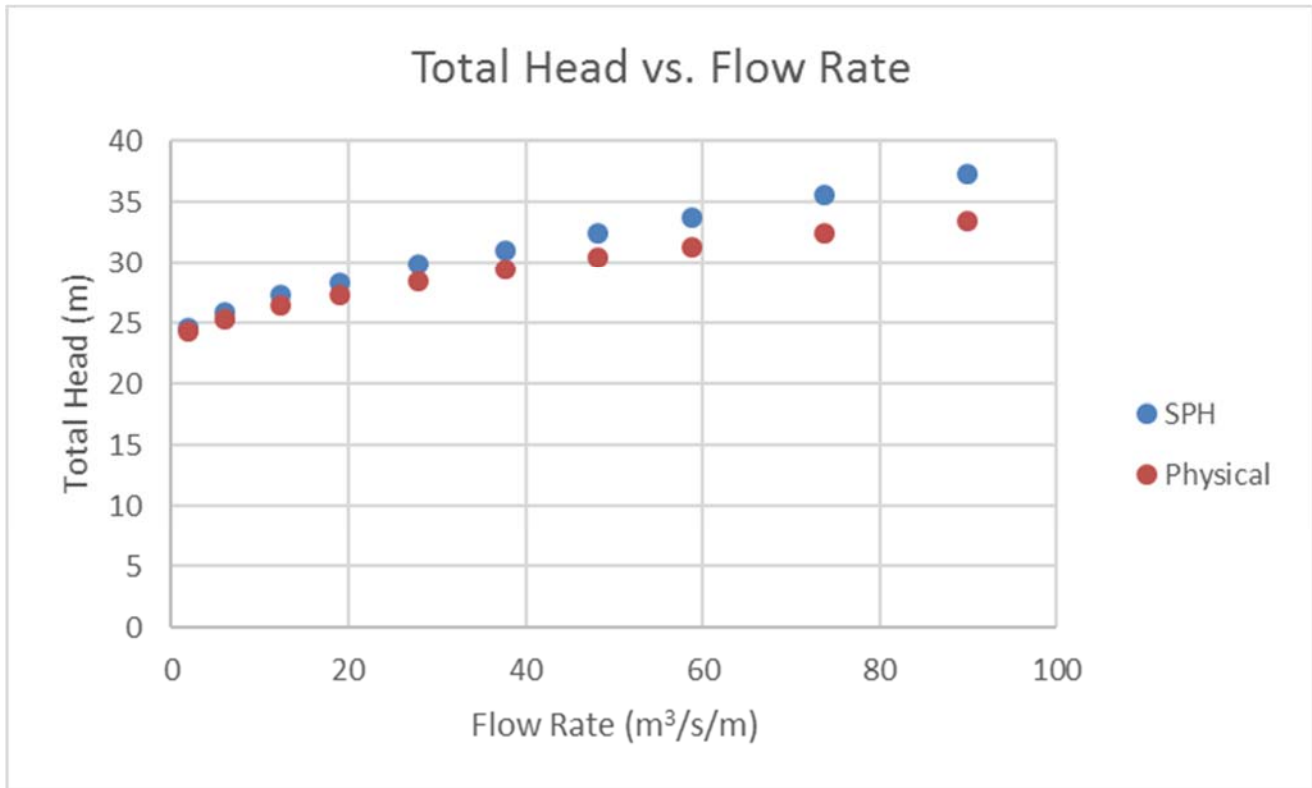


Figure 23. Total head vs. flow rate plot.

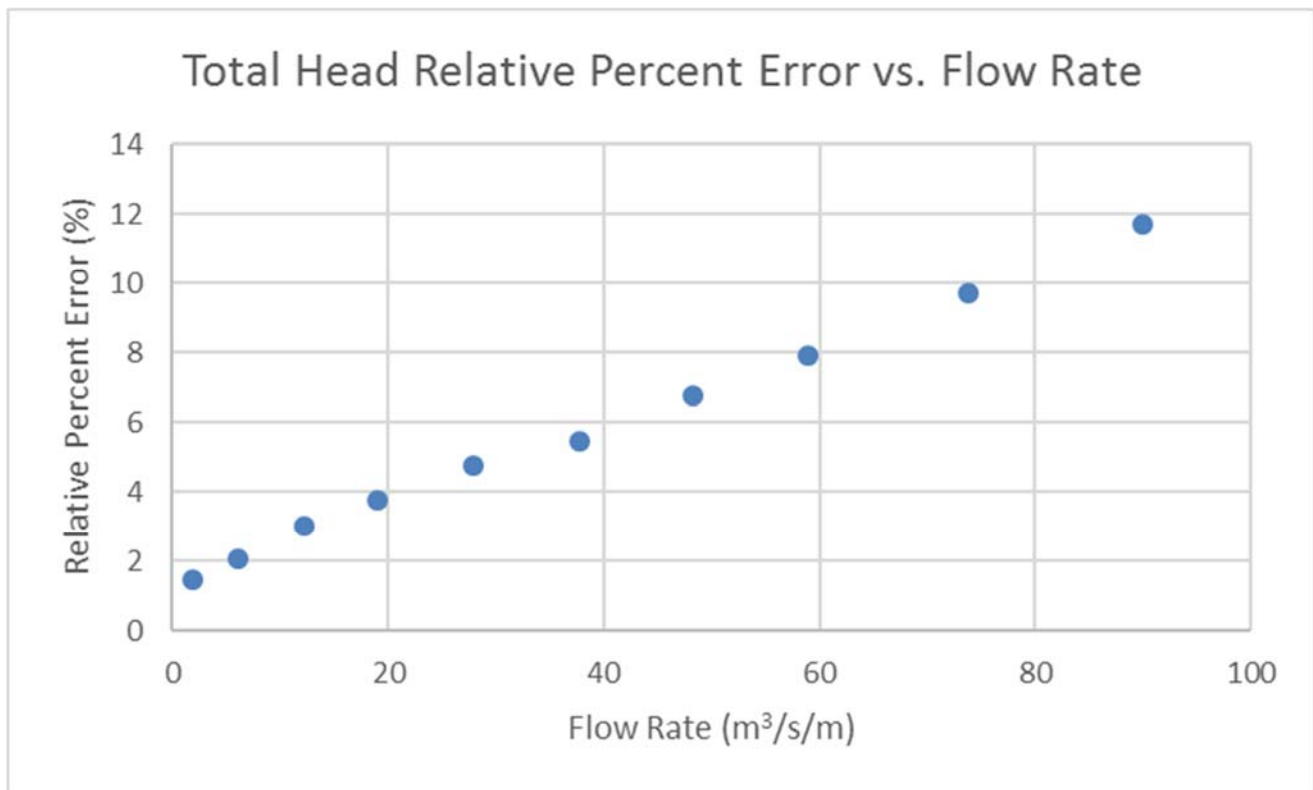


Figure 24. Total head relative percent error vs. flow rate plot.

The results show that SPH provided results within 12 % of the physical results for all ten runs. The results also show that the relative percent error increased as the flow rate increased. This means that more work needs to be done on model optimization. While the 4-m model width and 0.35-m particle diameter provided close results at the lower flow rates, it did not provide results as close at the higher flow rates. Therefore, more work needs to be done to determine the appropriate particle diameter given a width and flow rate. The ogee spillway model optimization and comparison results were submitted to the *Journal of Fluid Mechanics* on July 12, 2017 for publication and is currently under review.

One area that needs more work is how to determine the appropriate particle diameter. This comparison has shown that particle diameter is dependent, at the minimum, on geometry and flow rate. The results showed that the optimized model provided results within 1.45 % at the low flow rate, but the error continued to grow as high as 11.74 % as the flow rate increased. Since SPH can provide low error results at low flow rates, it should be able to provide low error results at high flow rates given the appropriate particle diameter. Therefore, more research needs to be conducted to determine the appropriate particle diameter given parameters such as geometry and flow rate.

To determine the appropriate particle diameter given certain parameters, the SPH code Neutrino is being coupled with the Risk Analysis Virtual Environment (RAVEN) code. RAVEN is capable of running external codes and performing parametric and probabilistic analysis based on the results of the external codes [8]. By coupling RAVEN and Neutrino, the goal is to use RAVEN's optimization and statistical analysis abilities to help determine the appropriate particle diameter for different scenarios.

To achieve the Neutrino/RAVEN coupling, a Neutrino interface needed to be coded so that RAVEN can run Neutrino. The Neutrino interface is a python class that consists of five functions. Two of the functions are used to check the input file, one function creates new Neutrino input files, one function generates the command to run Neutrino, and one function moves and converts the Neutrino output so that RAVEN can interpret the results.

Once the Neutrino interface was created, a RAVEN input file could be created to test the Neutrino/RAVEN coupling. To test the coupling, a simple Neutrino simulation was created. The simulation consists of a block particle emitter inside a rigid box and a measurement field which measures the number of particles in the field. Figure 25 shows the setup of the simulation.

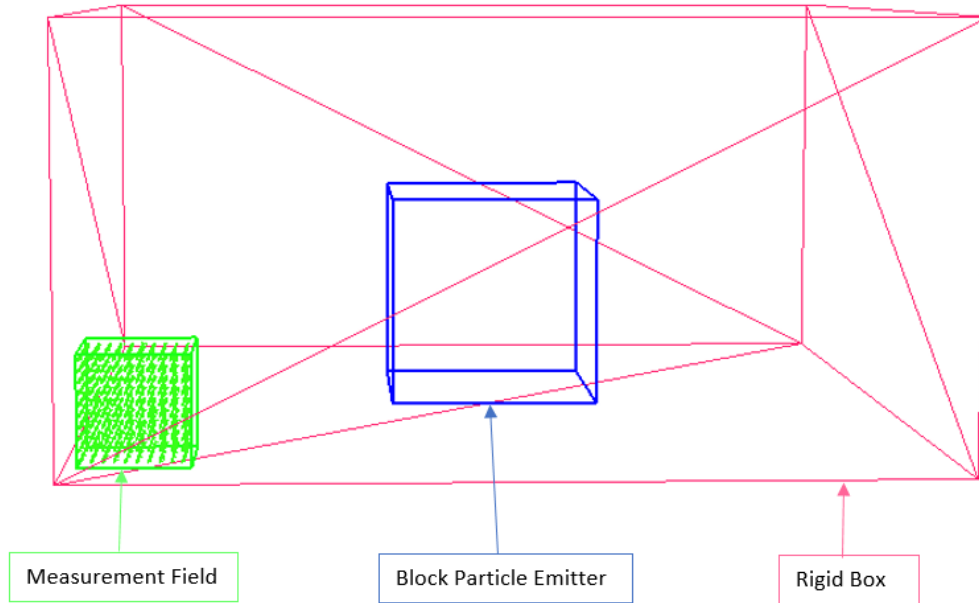


Figure 25: Neutrino/RAVEN coupling test simulation setup.

Next, a RAVEN input file needed to be created. The RAVEN input file for this simulation consists of stating the Neutrino input file name, instructing RAVEN to use the Neutrino interface, creating a uniform distribution and a Monte Carlo sampler, creating data objects for the results, and instructing RAVEN to plot the results. The uniform distribution and Monte Carlo sampler are used to choose different particle interaction radii which in turn adjusts the particle diameter. The details for this simulation consist of a uniform distribution with a range between 0.1 and 0.6 with the distribution being sampled 5 times. Other distributions, samplers, and values can be used, but these are what were used for testing.

Once the RAVEN input file was created, the simulation could be run. The Neutrino/RAVEN process consists of checking and reading the RAVEN input file, sampling the distribution to select new particle interaction radii, creating new Neutrino input with the sampled radii, generating and executing the commands for each Neutrino run, collecting the output from Neutrino, and plotting the results. The RAVEN plot, Figure 26, shows the number of particles vs. time for five different particle interaction radii which is denoted by the color map.

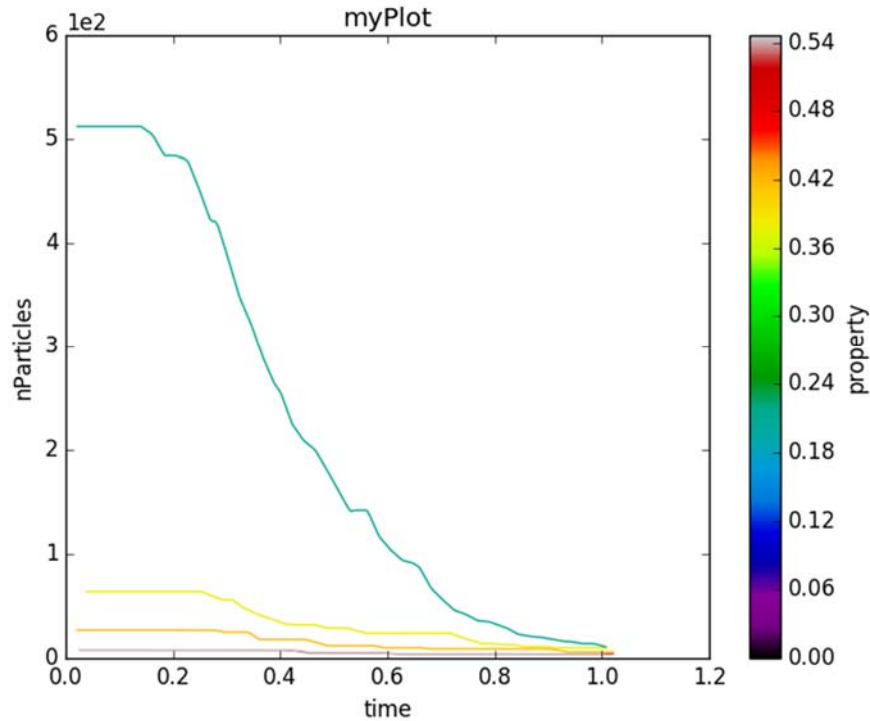


Figure 26: Neutrino/RAVEN coupling test plot.

At this point, RAVEN and Neutrino are coupled. RAVEN can edit the Neutrino input file, run Neutrino, and read and plot the results. However, work is still being done on statistically analyzing the results from Neutrino as well as creating clear plots. Additionally, more work needs to be done to remove any hardcoded information that was put into place while testing.

The next step is to implement RAVEN's optimization tool so that RAVEN will optimize the particle diameter for different scenarios without the user having to change the parameter. After the optimization has been tested with the Neutrino coupling, the particle diameter for the high flow rate ogee spillway comparison run from above will be optimized using RAVEN to determine what particle diameter is needed. This will help determine if using a smaller particle diameter than 0.35 m will provide a result closer to the physical result.

With Neutrino and RAVEN coupled, different scenarios can be run to help determine a method for selecting particle diameter without the user having to change the input file and wait for runs to finish. This will allow for a more efficient approach.

Once a method for determining particle diameter is identified, more comparisons and test cases need to be performed to verify that method. After that has been done, SPH should be considered reliable for the modeling of flooding scenarios. The end goal will be to incorporate flooding failure data into an SPH code or to couple an SPH code with a risk assessment code. This will allow for flooding scenarios to be modeled so that the damage of a flooding event can be determined before it happens. It would also identify actions that need to be taken to reduce the damage.

Additionally, preliminary SPH simulations have been constructed to explore the ability of Neutrino to incorporate failure properties of structures. In one such simulation, a rectangular room with two interior walls was created as shown in Figure 27 below. Both interior walls were fashioned with rectangular openings. These openings were then filled with rigid cuboid structures to simulate a door.

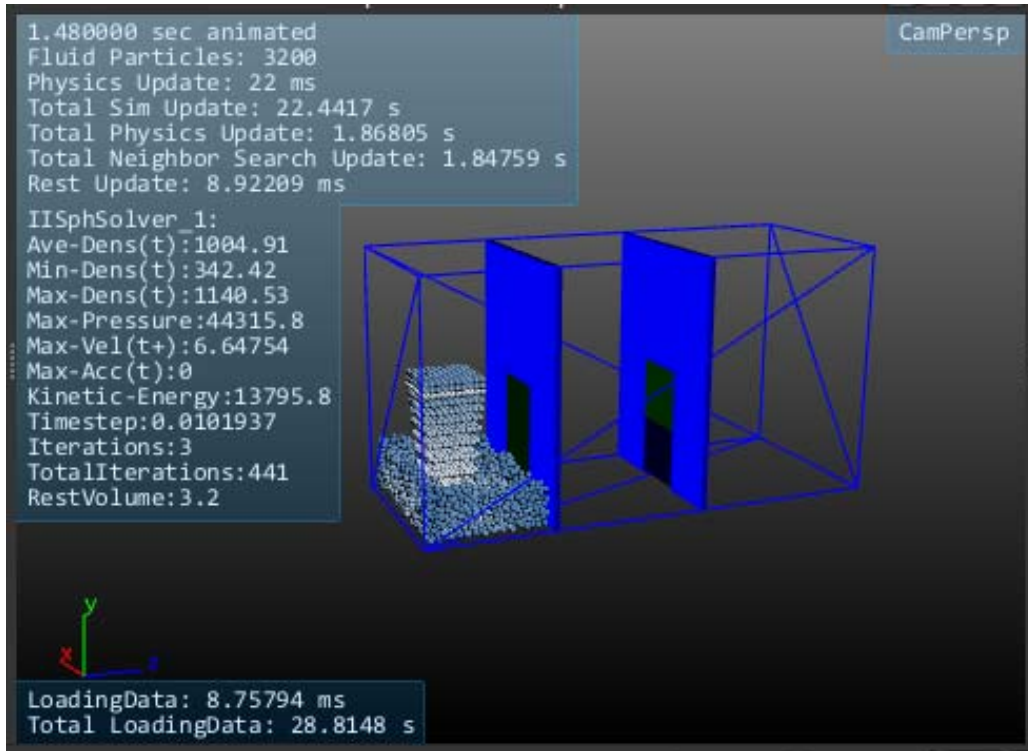


Figure 27. Initial sequence of force driven door failure experiment.

A square particle emitter was activated to fill the first of the three rooms with particles. Custom Python code was imbedded into Neutrino to calculate and record the force exerted on the first door with each time step. The first door was programmed to translate upward when it experienced a given fixed force of 4000 N. Figure 28 shows the translation of the first door simulating the failure.

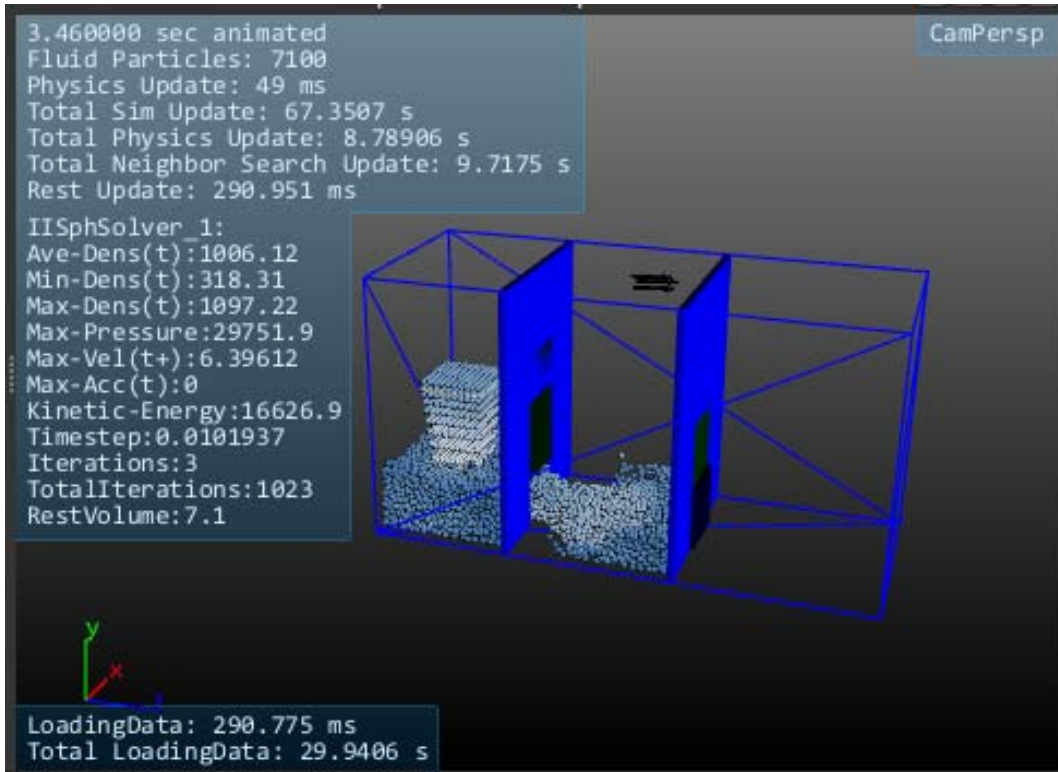


Figure 28. Failure of the first door after 4000 N was exerted by the build-up of particles behind it.

The second door in the failure sequence was programmed differently. The Python code imbedded into Neutrino changed the door structure type from static to dynamic allowing the door to release from the framework of the wall and respond to gravity, buoyancy, and the forces exerted by the particles. Figure 29 shows the failure of the second door in the sequence as it responds as a dynamic object.

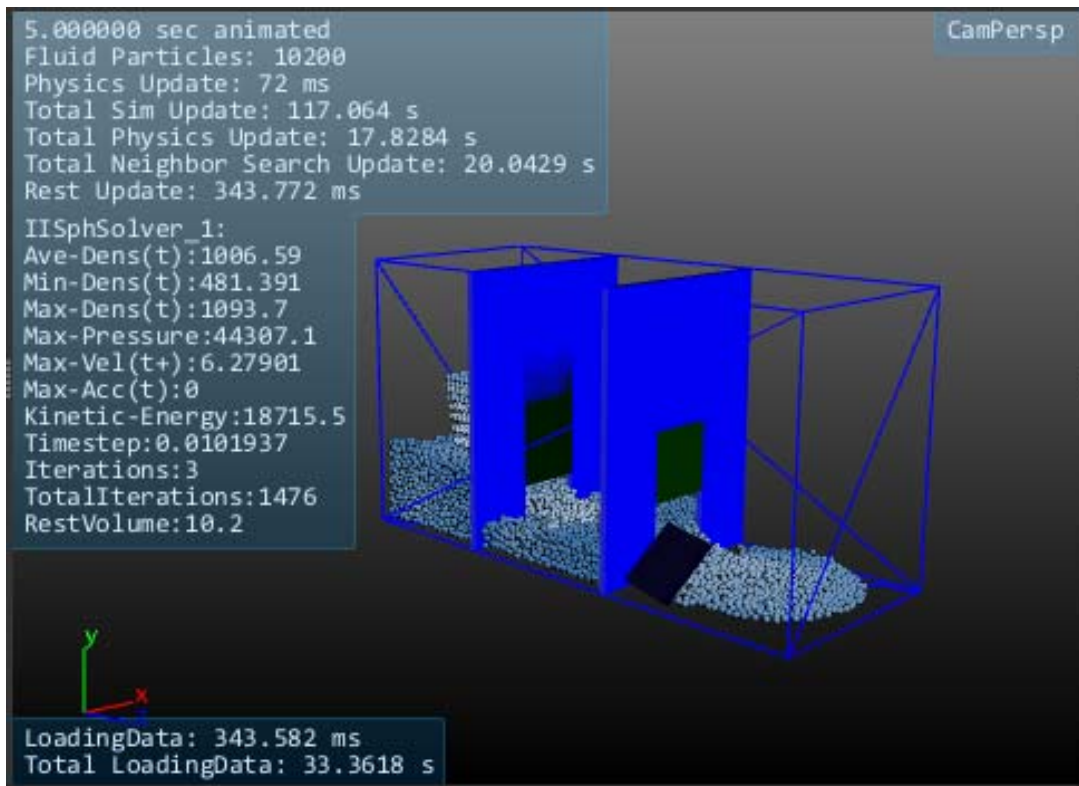


Figure 29. Failure of the second door showing the change from static to dynamic object type.

This failure experiment was developed with hard-coded failure modes based on the forces experienced by the doors. Future simulations will explore the ability of Neutrino to incorporate probabilistic failure modes based on the physical experiments and data obtained from the PET experiments.

8. WAVE IMPACT SIMULATION DEVICE DESIGN

The status of wave impact research and preliminary Wave Impact Simulation Device (WISD) designs are presented in this section. The WISD will provide wave impact testing capabilities for CFEL and information collected from wave impact testing will be applied to risk modeling studies.

A literature review of tsunami and ocean wave research was conducted with an emphasis on wave impact studies. The research included wave theory and idealized wave behavior, representative waveforms of natural waves, wave impact studies, artificial wave generation systems, and software wave simulation methods. It was found that wave research has generally targeted idealized wave behavior, methods of simulating waveforms numerically, and artificial wave generation. Wave impact studies often consider a structure of interest, such as a sea wall or pier, under specific wave impact conditions. Empirical methods are used to provide a method of predicting wave impact forces. To generate artificial waves, wave flumes and basins are the most common methods. These facilities use wave paddles and other displacement techniques to produce artificial waves generally at a model scale.

Numerous numerical techniques have been applied to model wave behavior, and the computational fluid dynamics (CFD) approach has been applied to this project. To simulate full scale wave impacts on prototype components and structures, the CFD code Flow-3D was used to model large tsunami wave impacts. Natural wave

behavior is influenced by parameters such as fluid depth, ocean floor, coastline topography, and wavelength. The complex interaction of these parameters produces a vast range of wave conditions.

To provide a method of simulating wave impacts for CFEL, idealized wave behavior was assumed to simplify the wave impact conditions. Only non-breaking wave velocities can be described by idealized wave celerity. It was proposed that the maximum horizontal fluid velocity for a specified wave shall be determined from the idealized wave equation for non-breaking wave conditions. By considering only non-breaking waves, horizontal fluid velocities control the impact force of the wave, and vertical velocity components can be deemed negligible.

Tsunami wave impacts were investigated to represent a worst-case scenario, and constant approach geometry is used in Flow-3D simulations. The idealized wave velocity, which is dependent on wavelength and fluid depth [9], is defined as

$$c = \sqrt{\frac{g\lambda}{2\pi} \tanh\left(2\pi \frac{d}{\lambda}\right)}$$

where c is the wave celerity, λ is the wavelength, d is the fluid depth including the wave height, and g is the gravitational acceleration on earth.

The idealized wave velocity equation can be modified at the boundary conditions of the hyperbolic tangent term by comparing the wavelength to the fluid depth. If the fluid depth is greater than half of the wavelength, the wavelength controls the celerity only, and is described as a deep-water wave. Wind driven waves are the most common type seen in nature, and are classified as deep-water waves.

When the wavelength is greater than the fluid depth by a factor of 20 or more, fluid depth solely governs the equation. This flow regime is deemed shallow water wave behavior. Non-breaking tsunami wave celerity is described by shallow water theory [9]. The simplified wave celerity equation for shallow water waves is defined as

$$c = \sqrt{gd}$$

where c is the wave celerity, g is the gravitational acceleration on earth, and d is the fluid depth including the wave height.

By defining a tsunami wave as a shallow water wave, a maximum horizontal fluid velocity of 25.4 ft/s for a wave height of 20 ft was obtained. This maximum velocity was used to determine the necessary capabilities of the WISD. To meet the goals for CFEL testing capability, a wave section 10-ft wide by 10-ft high with a controlled profile must be produced.

Using Flow-3D, the 20-ft tsunami waves were simulated as solitary waves, and the impact forces caused by the waves were recorded for fixed approach geometry. In each simulation, a 20-ft high solitary wave traveled from left to right in a body of water with a constant 20-ft depth and approached a 10-degree slope leading to a horizontal beach. To reduce computational time, the simulations were designed as sectional models; a thin slice of an infinitely wide wave perpendicularly approaching a shoreline. This effectively creates a 2D model that is valid because the flow variations parallel with the beach are not significant. Figure 30 shows the Flow-3D solitary wave simulation. The impact force on a small baffle located on the beach at various locations provided insight into how the wave impacts structures and recorded the effective force of the wave based on what section of the wave impacts the baffle. Figure 31 shows the imminent impact of the solitary wave on a baffle.

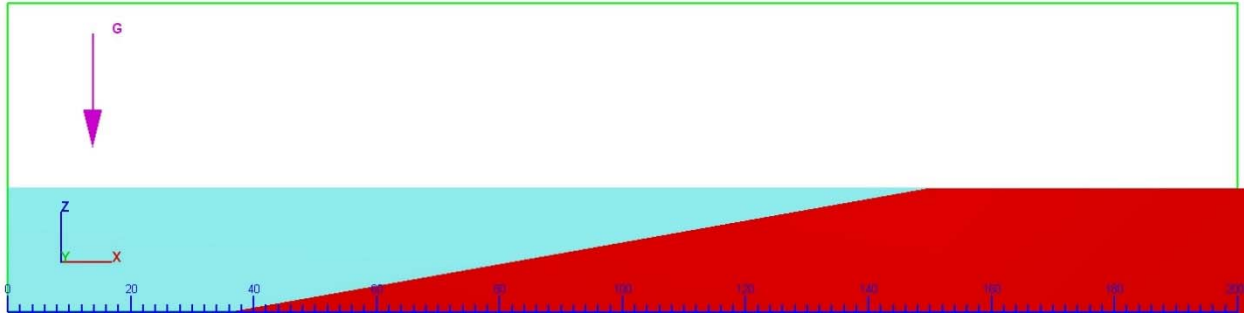


Figure 30. 20 ft solitary wave Flow-3D simulation (X-Z Plane).

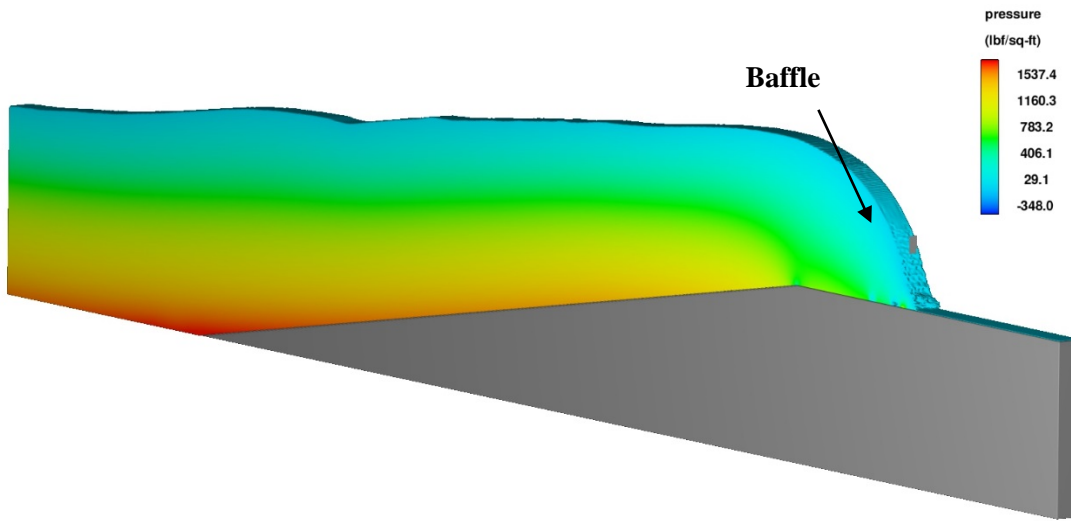


Figure 31. Isometric view of wave pressures at imminent baffle impact.

The impact forces recorded in the Flow-3D solitary wave simulations were found to have high variability in the impact zone of interest with the location of the baffle greatly influencing the results. It was observed that the variability in results occurs when the waveform loses stability and the flow becomes more turbulent. It was concluded that the approach of identifying the impact force caused by a wave for all possible impact locations was not practical, even if the simplified scenario used in the sectional solitary wave simulations was the only scenario studied. The results only applied to the simplified geometry used in the sectional wave simulation and could not be used to accurately predict wave impact forces in different scenarios.

A key restriction in the WISD design process is the limited lab space and funding available. As a result, artificial wave generation systems such as wave basins and flumes are not viable solutions due to inherent wave height restrictions in open channel flow. Instead of generating an artificial wave for impact testing, a high velocity jet was proposed as an alternate means of simulating a high velocity wave impact. By producing a fluid jet with a near vertical profile exiting the 10-ft wide by 10-ft high conduit, a 1- ft wide section of a 10-ft high wave can be imitated. For wave heights greater than 10 ft, the wave section will represent the base of the wave with the corresponding wave speed.

Flow-3D was also used to design a device capable of simulating these impacts. To design a WISD to be used in CFEL wave impact tests, the velocity and momentum of a tsunami wave with a maximum height of 20 ft must be matched, and a near vertical 10-ft by 10-ft section of water must be generated for impact tests. Achieving both

goals will allow large components or structures to be subjected to impact forces equivalent to a full-scale wave of varying height and velocity. Tsunami wave celerity is approximated using shallow water wave equations.

A multitude of models were simulated in Flow-3D to determine an ideal design for a WISD capable of creating a near vertical wave section with the same velocity as a 20-ft tsunami wave. Flow-3D models exploring vertical and horizontal pistons displacement mechanisms were investigated, as well as designs using air pressure to displace fluid.

A WISD design obstacle identified in the computer modeling of solitary waves was gravitational acceleration. Fluid was pulled towards the bottom of a wave profile as the waveform loses stability, creating an advanced fluid front at the base of the advancing wave section. Although a small advance front or tongue is present in natural waves, the slope of the wave face produced by the WISD must be controlled to produce realistic wave sections for impact testing. To counter this behavior, horizontal plates were placed at 1-ft height intervals in the conduit, dividing the 10-ft high wave section into ten 1-ft sections. As a result, gravity could not pull water from the top of the conduit to the bottom inside the exit conduit.

Numerous design iterations were required to investigate the use of pistons to displace fluid in the WISD. The final iteration, Design F, is shown in Figure 32. A vertical gate system is used to contain the fluid stored in the reservoir. Once a test is initiated, the gates rotate to allow fluid into the conduit, as shown in Figure 33. A piston at the back of the reservoir then pushes the fluid out of the reservoir at a specified velocity. The fluid enters the conduit, supported by the horizontal plates in the conduit, and exits with the profile shown in Figure 34. The resulting wave section was cohesive, near-vertical, and had a velocity profile very close to the target velocity of 25.4 ft/s.

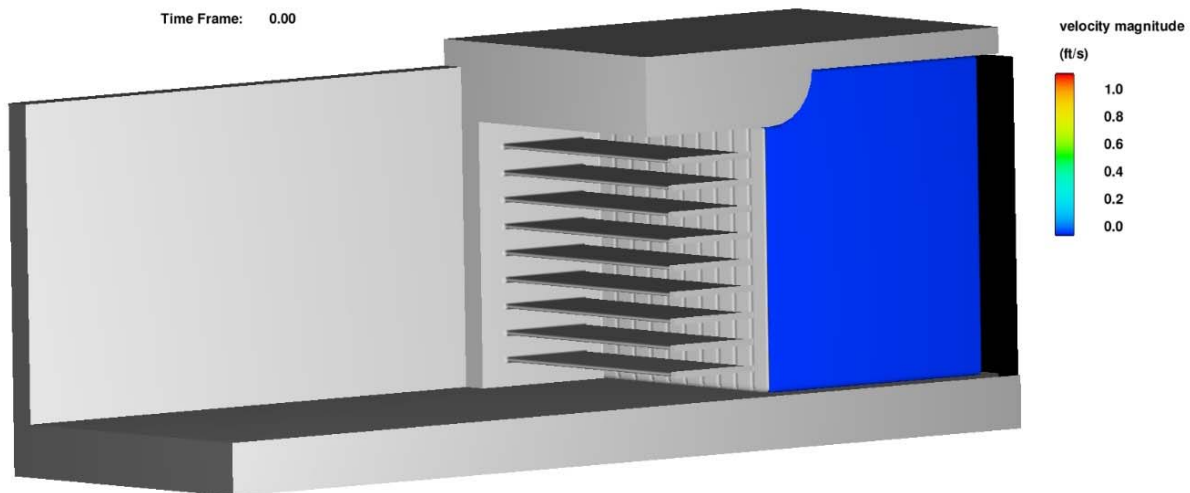


Figure 32. Design F isometric view.

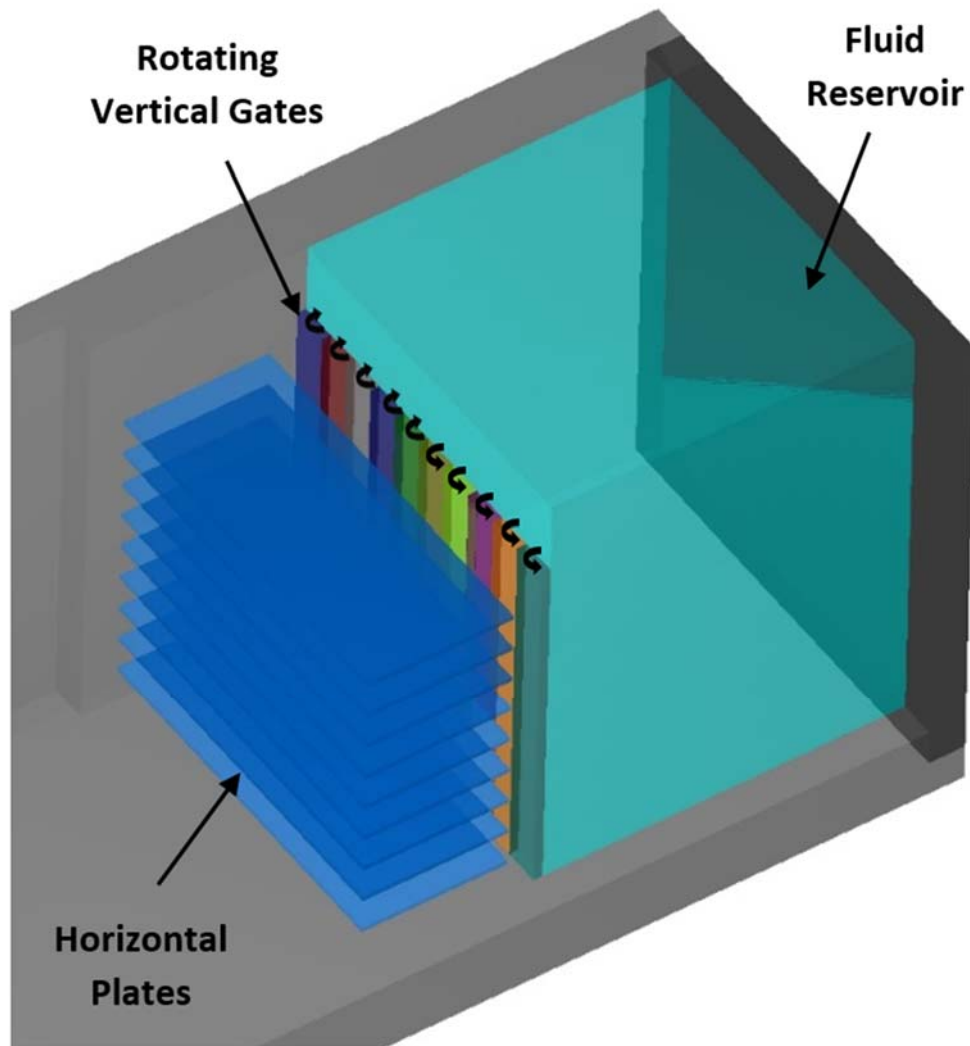


Figure 33. Design F gate system: isometric view.

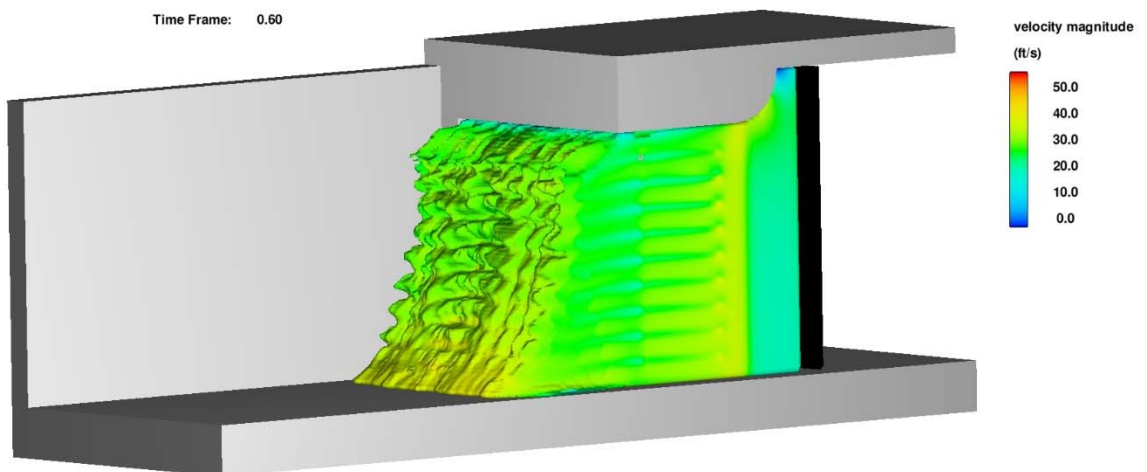


Figure 34. Design F isometric view: wave section profile.

The other method of fluid displacement explored in the final design iterations was air pressure. Figure 35 shows the isometric view of Design J, the final design developed for an air pressure displacement design. The horizontal plates that support fluid in the exit conduit are extended to the back of the reservoir, separating the entire conduit in ten discrete channels. Plates angled at 45 degrees at the back of the conduit create a free surface at the back of each channel for air pressure to act on. A horizontal gate system is used to contain the fluid stored in the reservoir. Once a test is initiated, each gate rotates about its own base towards the conduit exit. Air pressure acts on each fluid channel, pushing fluid out of the system at a specified velocity.

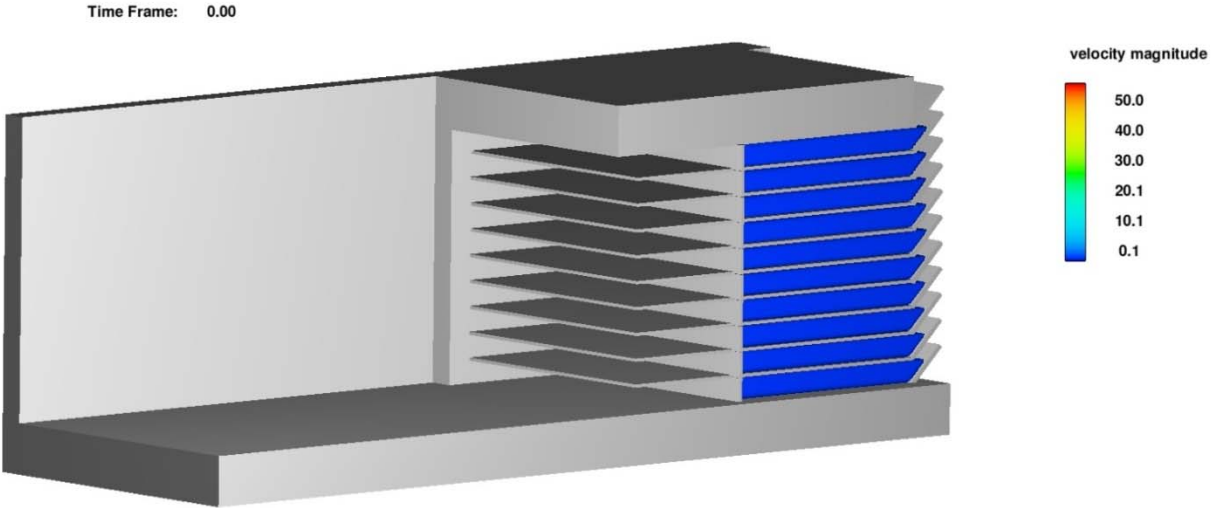


Figure 35. Design J isometric view.

Figure 36 displays the resulting wave section of the simulation. The wave section produced by Design J was cohesive, near-vertical, and had a velocity profile very close to the target velocity of 25.4 ft/s.

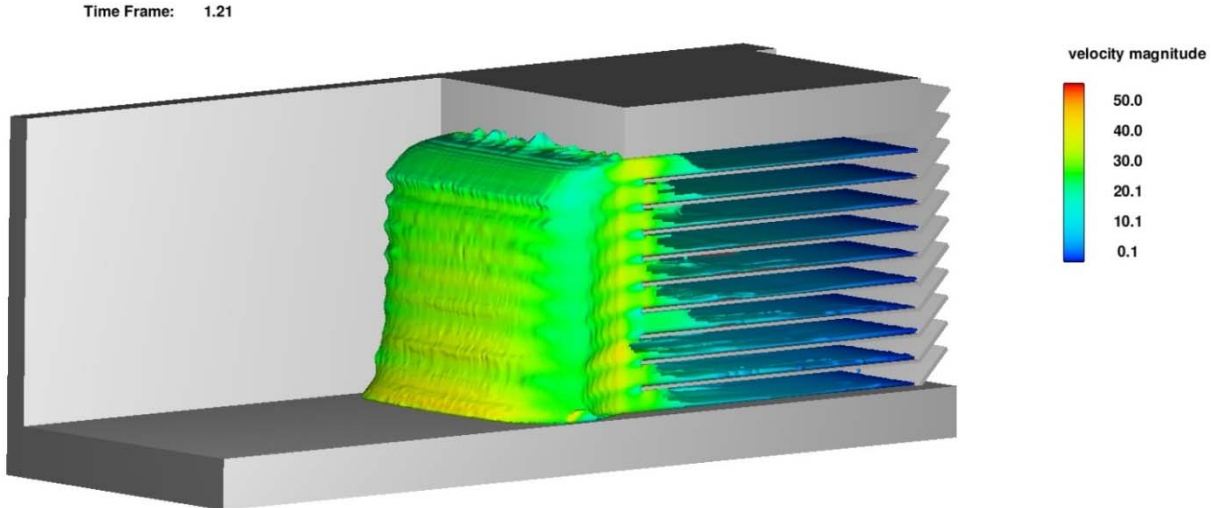


Figure 36. Design J isometric view: wave section.

To meet the CFEL testing goals of producing a near vertical wave section capable of simulating the impact of wave heights up to 20 ft, Designs F and J were the most promising for a plate driven and an air pressure driven option, respectively. Additional work is needed to evaluate the most effective design through prototype testing, and to determine the practical option to provide wave impact testing capability for CFEL.

An advantage of the air pressure design is the separation of the fluid depth into discrete channels. By doing this, various flow depths can easily be produced for impact tests. For flow depths less than 10 ft, the appropriate channels can be filled and operated. For flow depths greater than 10 ft, differences in air pressure in the discrete channels can be used to adjust the slope of the wave section and produce a desired flow pattern. For this reason, Design J is proposed as the most viable option for validation and further study. Design J also produced the most cohesive, vertical wave section.

Current work includes ensuring the validity and feasibility of the WISD designs. Scaled physical model testing of prototype designs will help identify potential design flaws, unexpected flow behaviors or unidentified design obstacles.

CFEL has effectively conducted CFD numerical simulation for the WISD conforming to the expectations of the study, but there is still uncertainty in the implementation of the WISD. While it is easy to implement a numerical boundary or an applied force, in the prototype there are still many unknowns. The primary concerns are the motive force and the gates. The motive force needs to accelerate the fluid quickly, and then maintain a steady fluid velocity. The gates need to seal the water prior to motion and then open rapidly allowing the water to move past with little interference.

The physical model will allow both the gate and motive force systems to be investigated, exploring both the flow behavior and the mechanical components. Although physical model parameters are still under review, current values are presented in Table 13.

Table 13. Physical Modeling Parameters

Model Scale Ratios and Prototype Equivalence		
Scale	Scale Value	Model to Prototype Equivalence
Length scale	$L_r = 5$	1 ft = 5 ft
Time scale	$t_r = 2.24$	1 s = 2.24 s
Velocity scale	$V_r = 2.24$	1 ft/s = 2.24 ft/s
Pressure Scale	$P_r = 5$	1 psi = 5 psi
Design Parameters (For small scaled Model)		
Scale factor		1:5
Prototype-Model Similarity		Froude Number
Velocity		11.36 fps
Pressure		125 psf (0.868 psi)
Materials to be used (Model)		
Outer walls		Plexiglass
Inner plates & gates		Steel

Preliminary gate designs have been discussed and explored. To achieve a suitable gate design, four major requirements have been identified as follows:

- Gates must be designed to withstand high water pressures prior to wave release
- Gate design should not interfere with the target flow profile
- All gates must open almost instantaneously
- Leakage should be kept at a bare minimum

Designing a gate system capable of meeting all four requirements presents a unique challenge; however, the leading solution that is being investigated involves the use of a slim butterfly valve gate coupled with an electromagnetic locking mechanism. In this system, the shaft of the butterfly valve gate extends to the outside of the WISD where it is connected to the strike plate of the electromagnet. While connected to a power source, the electromagnet provides twice the holding force required to hold each gate tightly closed while water pressure builds in the reservoir section. The moment power to the electromagnet is cut, the fail-open mechanism allows the gate to swing open freely. To maximize the angular velocity of the gate to its final position, a helical spring is connected to both the strike plate and a shock-absorbing stopper. Leakage will be addressed using gasket material applied to the perimeter of each gate.

A computer simulation of the proposed system is shown in Figure 37 and Figure 38. A scaled physical model is also currently underway.

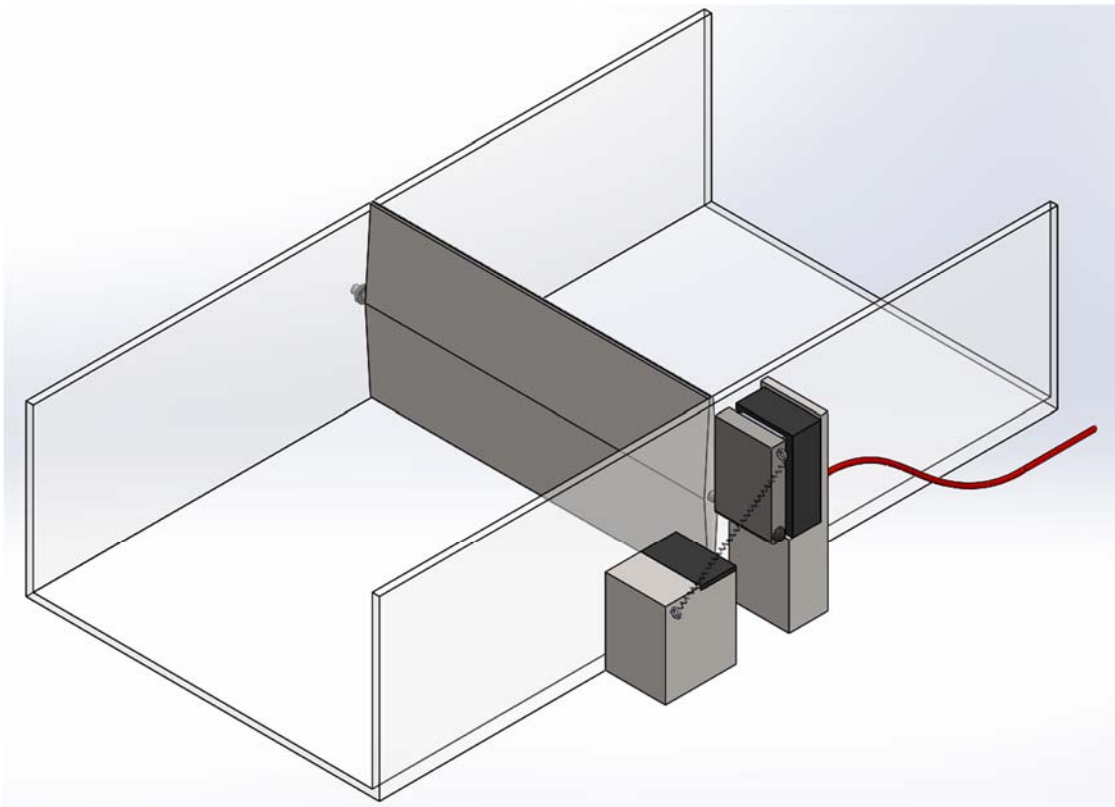


Figure 37. Scaled model of system with gate closed (power to electromagnet on).

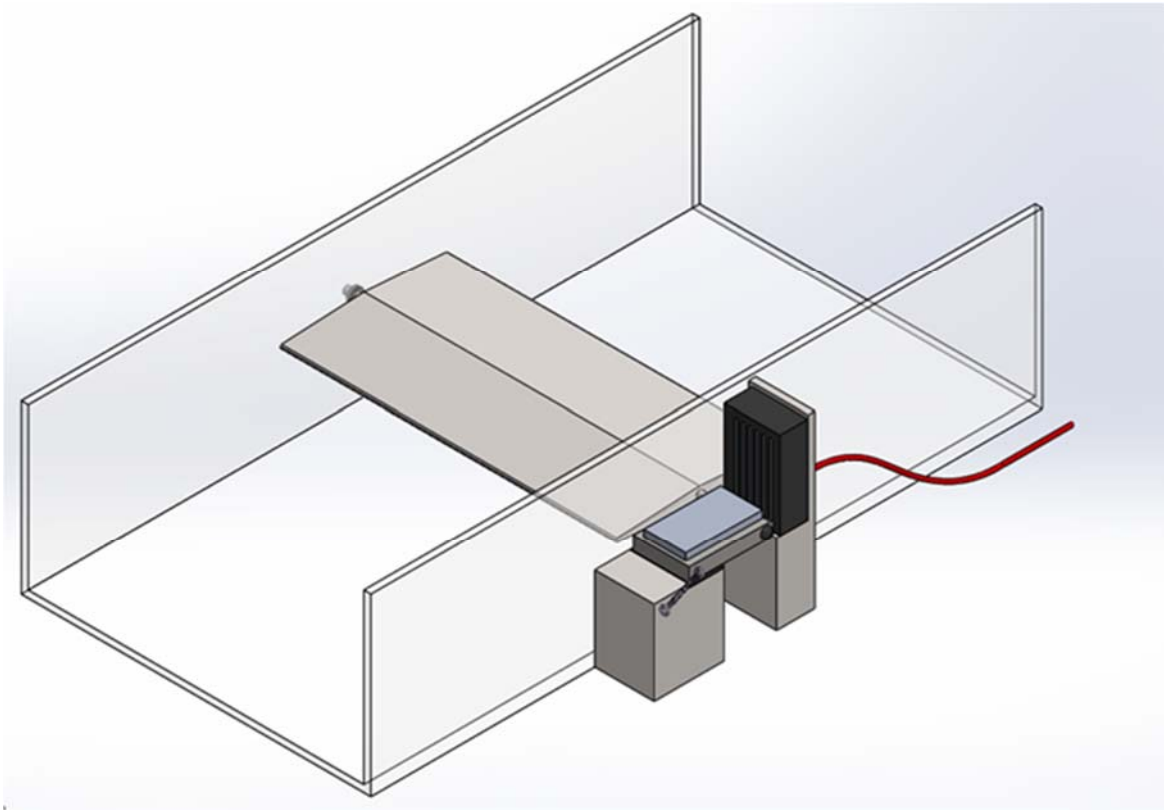


Figure 38. Scaled model of system with gate open (power to electromagnet off).

Research on the WISD continues forward simultaneous with numerical solutions and design of physical models. The numerical simulations are being performed using the CFD software, Flow-3D, with a focus directed on the motive force. As determined in previous research, the motive force needs to provide a large force to initiate motion in water and then reduce to maintain a steady fluid velocity. To reduce the computational time to compute a transient motive force, a sectional model was constructed using only one section of the jet. In addition, modifications to the section have been completed, looking for the most effective arrangement to apply air pressure to displace the water by considering differently angled inlets and fluid depths. Table 14 shows the various simulations that have been completed. Figure 39 shows the initial setup for an inlet inclined at 45 degrees with a depth of 1 foot with Figure 40 showing an inlet inclined at 25 degrees with a depth of 2 feet.

Table 14. Various simulations conducted in FLOW 3D

Inlet Angle Depth	45 degrees	35 degrees	25 degrees
1 foot	✓	✓	✓
2 feet	✓	✓	✓
3 feet	✓	✓	✓

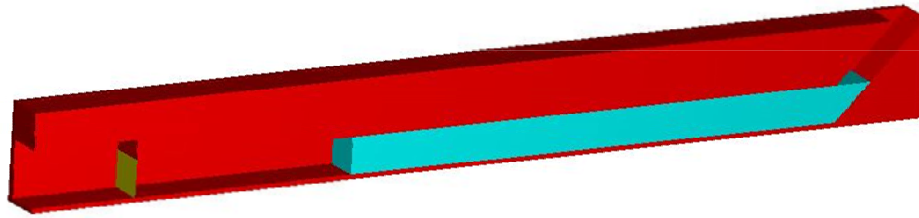


Figure 39. Section of WISD - Inlet angle of 45 degrees and a fluid depth of 1 foot.

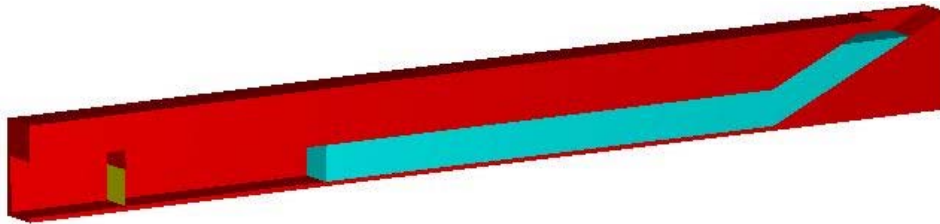


Figure 40. Section of WISD - Inlet angle 25 degrees and a fluid depth of 2 feet.

To measure the flow rate exiting the chamber, a baffle was placed at the same location for all arrangements. These numerical baffles do not impede or change the flow, rather they are used to better understand the fluid behavior. The yellow component on the left end in Figure 39 and Figure 40 shows the location of the baffle. The motive air pressure was set to 625 psf. (lbs/ft²) for the simulations from an initial time, $t = 0$ second to 1.5 seconds; 1.5 seconds being the total time of the simulation. The mass flux for several arrangements were recorded with respect to time and compared in Figure 41. The simulation configurations included inlet angles at 25 and 45 degrees with upstream depths ranging from one to three feet. All the simulations had similar behavior; the mass flux would sharply increase at 0.7 seconds and then gradually increase for a range from 0.8 seconds to 1.3 seconds followed by a sudden decrease as the water exited the flow chamber.

Comparing the one-foot depth inlet for angles 25 and 45 degrees, the results shows that the inlet angle does increase the motive force, moving the water through the chamber with a slightly higher initial response at 0.8 seconds and a larger peak at 1.1 seconds. This was expected since the initial pressure force is pressure multiplied by the area and the 25 degree inlet provides more area. The figure also shows that increasing the inlet depth slows the initial response at 0.7 seconds but produces a higher peak that is delayed. The higher peak is attributed to the increase in the initial inlet depth and the time delay is created by the change in inertia required to move the additional mass.

Although these simulations provide good information on the behavior of the motive force, one of the goals of the WISD is to have a near constant mass flux for some section of the time frame, which did not occur. To modify the flow behavior, at approximately 0.8 seconds, the motive air pressure was varied to decrease sharply starting from 0.8 seconds. This was completed on one simulation with an inlet depth of one foot and a 45° angle. The variable inlet air pressure is shown in Table 15. The results with the variable pressure are shown in Figure 41. The results conformed with the expectations of the WISD, providing a nearly constant mass flux from 0.8 seconds to 1.2 seconds. Additional studies are underway to adapt analytical theories from literature to compute the ideal variation in the air pressure. Consecutively, the different geometries and fluid depths will be tested using the variable air pressure to further refine the concept.

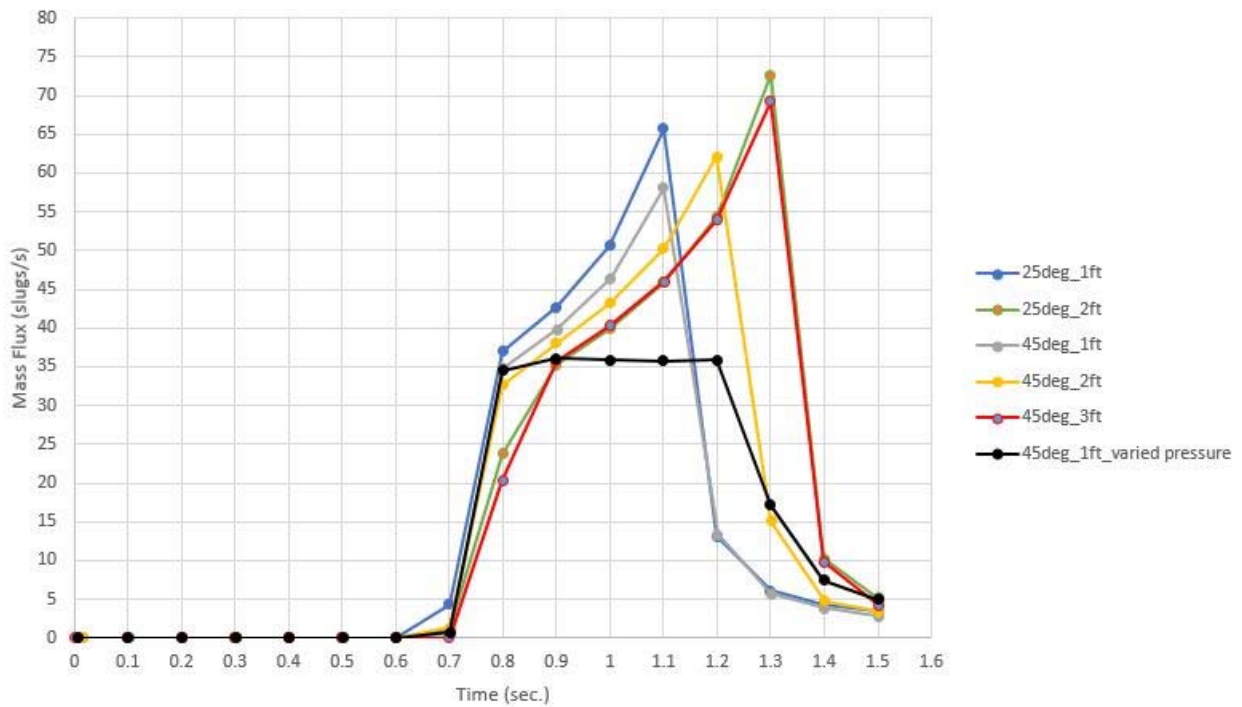


Figure 41. Mass flux vs time.

Table 15. Variable Pressure Boundary

Time (secs.)	Pressure (psf.)
0	625
0.3	625
0.6	625
0.8	625
0.9	75
1.2	50
1.5	0

9. PIPE LEAK RESEARCH

The research for this project will be a part of one of the three types of water impact tested with CFEL. The PET is currently used for water rise, the WISD will be for wave impact tests, and this research will begin the water spray portion. The scope of this project will be experiment design and database building. The plan is to cause pipes to fail by ruptures, record key variables and visual evidence, and build a database of results. A second database can be then linked with the pipe results that will compare how specific components fail under these spray accidents. Both databases can then be used in risk assessment modeling.

The first step of the experiment design will be to build the test section. After the modifications to the PET are made, this project will seek to take advantage of the PET as a testing space. The PET has two 3 in inputs at the bottom of the tank. These will be used for the test loop. The 3-in pump will be piped into the PET, then back out into the floor reservoir, with the test section inside the PET. On each side of the PET will be a flow meter to monitor the leak rate through the pipe crack. The leak rate through the crack at any instant will be the difference

between the readings of the two flow rates. The failure section may be an elbow, straight pipe, or a tee. Pressure gauges will be mounted upstream and downstream of the test section to measure the pressure drop across the failed section. The PET will not be sealed with a wall in these tests, but will be used primarily for controlling the water from the leaks. Lastly, there will be a wall painted in a checkered pattern behind the test section that, with the help of a camera, will be able to capture the spray pattern.

The results of these tests will then be recorded in a database that will record these key characteristics:

- The leak rate through the crack
- The pressure drop across the crack
- Pipe material and diameter
- Crack characteristics (location, orientation of pipe, longitudinal or circumferential, crack length, etc)
- Water exit velocity
- Water temperature
- Spray description

There may be a few obstacles with this experiment. One is temperature. The temperature of the water used may be much lower than seen in NPPs. This means that it will not be able to account for steam lines, or water/vapor mixture lines. Second, the amount of pipe failure configurations may be so large that a comprehensive database may not be possible. This research will lay out an experimental framework to fill in the database. The idea will be to have a living database that can be filled with information as requested by customers should they find information lacking.

One of the key ideas that is essential to this research, and nuclear power plant life, is leak before break (LBB). The concept states there should be more than the minimum detectable leak rate leaking from a pipe before catastrophic failure occurs or pipes should leak before they rupture. These leaks can range in size, the orientation of their stream, the exit velocity of the stream, crack characteristics, and more. One of the parameters that has been studied widely regarding leaks is how to measure their flow rates. This is due more to the concern of loss of cooling accidents occurring rather than component damage accidents.

Two ways to determine the leak rate through a crack are the Henry-Fauske model and the modified Henry-Fauske model. In Park et al [10], they use these models in a program estimating the leak rate through a crack. They show that the leak rates calculated in these models match closely at small crack lengths but diverge as the crack length grows.

This paper also mentions that the leak rate from a crack shows significant scatter from measured flow rates. The variables recorded in the experiment for this project may need to be recorded as mean and standard deviation if this is true. Park et al recreated this in their program by treating the crack characteristics as normally distributed random variables and performing a Monte Carlo analysis. Figure 42 shows the results of three of these simulations, where b is the half crack length. This plot shows that the leak rate through the crack is not linear with the crack length, which may end up being true for other factors, such as the pressure.

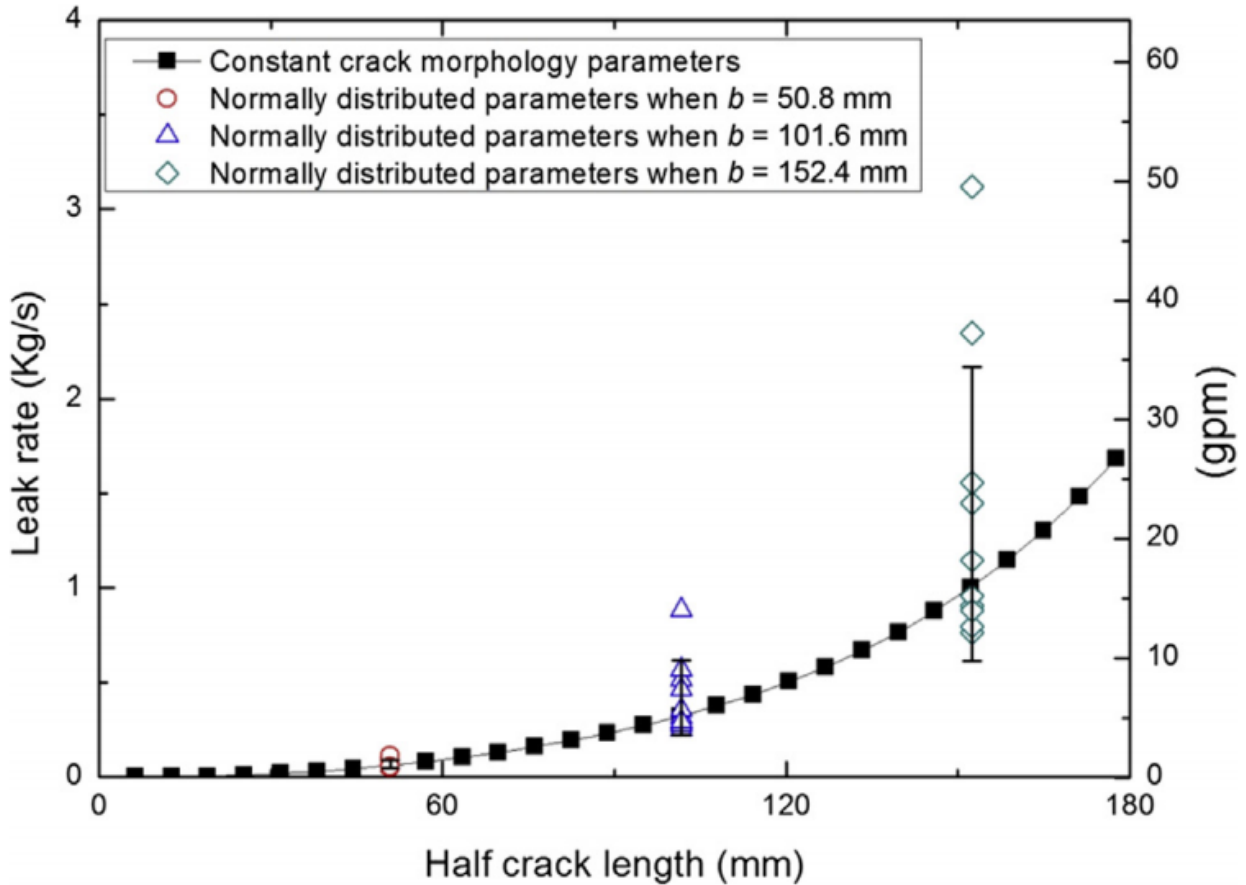


Figure 42. Leak rates for normally distributed crack morphology variables [10].

The Swedish Nuclear Power Inspectorate (SKI) performed a study of pipe failure events at United States NPPs from 1961-1995 [11]. This database examines several report databases. The three most important report databases are Licensing Event Reports (LERs), Abnormal Occurrence Reports, and Reportable Occurrences. These three are all used, or have been used, by the NRC, and the LERs have the most extensive set of event data. In all, this study aggregated 1,511 reports of piping failures in the US in the studied period, and created a Microsoft Access database for the events.

This study uses six different terminologies to define pipe failures. First is leak, defined as a limited but finite amount of water is released, varying from leaks of cubic centimeters per hour to a liter or more a minute. Next is crack/leak, defined as having finite depths and penetration of the pipe wall to create a leak, and is a subset of leaks. Next is failure, which in the context of these reports is a vague term as they do not use any quantifying terms. Several failures in these reports ended up being leaks after further assessment of these reports. The last three categories; rupture, severed, breakage, are used synonymously and center on holes the size of the cross section of the pipe to full double-ended guillotine breaks. Each failure in the database is defined by one of these terms to indicate the severity of the damaged piping.

The following tables show some categorical breakdowns of the data from the SKI database. Table 16 shows the numbers of failures sorted by pipe size. The first set of data, 1055 reports, is from the reports where the pipe size was reported in ranges: less than 1 in, 1 to 4 in, 4 to 12 in and greater than 12 in. Most of the failures were in pipes of size less than 1 in. The next set of data, 382 reports, is from reports where the exact size is unknown but it could be classified as either less than 1 in or greater than 1 in or a reducer. Lastly, it is reported that 74 of the

reports gave no indication of the pipe size. This shows that most pipe failures in the reporting period were in pipes of less than 1 in.

Table 16. SKI Report, Number of Piping Failures for Various Pipe Sizes and Pipe Size Categories [11]

Pipe Size/Category	Number of Failures
Actual Pipe Size	
≤ 1 inch	574
> 1 inch & ≤ 4 inches	252
> 4 inches & ≤ 12 inches	155
> 12 inches	74
Subtotal	1055
Pipe Size Category	
"<1"	227
">1"	142
Reducer	13
Subtotal	382
Unknown/Undetermined Size/Category	74
Total	1511

The next data table from the SKI report as seen in Table 17 shows the number of failures from the report based on the failure type. Failures from leaks were the largest category of failures. This is expected, as the LBB principle from before has described. It is these types of failures that will be examined in this research.

Table 17. SKI Report, Number of Piping failures by Type of Failure [11]

Failure Type	Number of Failures
Leak	
Leak	1274
Crack/Leak	54
Failed	64
Rupture	
Breakage	13
Rupture	76
Severed	30
Total	1511

Finally, Table 18 below discusses the failure mechanisms described in each report for each type of piping failure. This shows that the two biggest known causes of failure are Fatigue-Vibration (FV) and Erosion/Corrosion (EC). FV failure is mostly a contributor to 1-in pipes and smaller, which is mentioned in the SKI report but is not visible in any of the presented tables. Additionally, the report describes a downward trend in failures after 1983, contributed to by changes in reporting requirements and increased safety standards, in all areas except ruptures. This is due to EC being the main cause of ruptures. The experiments in this project will seek to recreate these two

failure types in tested pipes with machining. The characteristics of these piping failures and the specifics of their failures are not clear at this point and require further research.

Table 18. SKI Report, Number by Piping Failures for Each Failure Mechanism Category [11]

Failure Mechanism (Code)	Number of Failures
Corrosion/Fatigue (C/F)	14
Construction Defects/Errors (CD)	184
Design-Dynamic Load (DDL)	8
Water Hammer (WH)	35
Fatigue-Vibration (FV)	364
Erosion/Corrosion (E/C)	295
Stress Corrosion / IGSCC (SC)	166
Corrosion (COR)	72
Thermal Fatigue (TF)	38
Other (OTH)	43
Unknown Causes (UNK)	292
Total	1511

The experiments for pipe leakage will start with these failures in mind. The piping examined will have a nominal diameter of less than 4 in and will focus on FV and EC failure. Some ruptures will be studied, but leaks will be the focus. Lastly, the specific pipe material is needed. Early research indicates stainless steel pipes, but further research is required.

10. CONCLUSION

Progress has continued on Nuclear Power Plant mechanical component flooding fragility experiments and supporting research. The progress includes execution of full scale fragility experiments using hollow-core doors, PET capability improvement design and installation, design of experiments exploiting improved PET capabilities, fragility mathematical model development, SPH simulations and RAVEN coupling, wave impact simulation device design, and pipe rupture mechanics research.

11. REFERENCES

- [1] C. Smith, "Light Water Reactor Sustainability Program, Flooding Fragility Experiments and Prediction, INL/EXT 16-39963," INL.
- [2] OpenBUGS, "OpenBUGS User Manual," [Online]. Available: <http://www.openbugs.net/Manuals/Contents.html>.
- [3] R. Levy, "Chapter 8 Hierarchical Models," in *Probabilistic Models in the Study of Language*, 2012.
- [4] "Wikipedia," [Online]. Available: https://en.wikipedia.org/wiki/Deviance_information_criterion.

- [5] B. M. Savage and M. C. Johnson, "Flow over Ogee Spillway: Physical and Numerical Model Case Study," *Journal of Hydraulic Engineering*, no. August, pp. 640-649, 2001.
- [6] M. C. Johnson and B. M. Savage, "Physical and Numerical Comparison of Flow over Ogee Spillway in the Presence of Tailwater," *Journal of Hydraulic Engineering*, no. December, pp. 1353-1357, 2006.
- [7] "Neutrino Documentation," GitHub, [Online]. Available: <http://neutrinodocs.readthedocs.io/en/master/>. [Accessed 17 Sept 2016].
- [8] "RAVEN," INL, [Online]. Available: <https://raven.inl.gov/SitePages/Overview.aspx>. [Accessed 8 Sept 2017].
- [9] N. Mayo, "Ocean Waves-Their Energy and Power," *Physics Teacher* 35, 1997.
- [10] Jai Hak Park, Young Ki Cho, Sun Hye Kim and Jin Ho Lee, "Estimation of Leak Rate Through Circumferential Cracks in Pipes in Nuclear Power Plants," *Nuclear Engineering and Technology*, pp. Volume 47, Issue 3, Pages 332-339, April 2015.
- [11] S. Bush, M. Do, A. Slavich and A. Chockie, "Piping Failures in United States Nuclear Power Plants: 1961-1995 (SKI-R--96-20)," Swedish Nuclear Power Inspectorate, Sweden, 1996.